CELL BIOLOGY

# The ER chaperone calnexin controls mitochondrial positioning and respiration



**Tomás Gutiérrez[1], Hong Qi[2], Megan C. Yap[1], Nasser Tahbaz[1], Leanne A. Milburn[1], Eliana Lucchinetti[3], Phing-How Lou[3], Michael Zaugg[3], Paul G. LaPointe[1], Pascal Mercier[4], Michael Overduin[4], Helmut Bischof[5], Sandra Burgstaller[5], Roland Malli[5], Klaus Ballanyi[6], Jianwei Shuai[7], Thomas Simmen[1]***

**Chaperones in the endoplasmic reticulum (ER) control the flux of $Ca^{2+}$ ions into mitochondria, thereby increasing or decreasing the energetic output of the oxidative phosphorylation pathway. An example is the abundant ER lectin calnexin, which interacts with sarco/endoplasmic reticulum $Ca^{2+}$ ATPase (SERCA). We found that calnexin stimulated the ATPase activity of SERCA by maintaining its redox state. This function enabled calnexin to control how much ER $Ca^{2+}$ was available for mitochondria, a key determinant for mitochondrial bioenergetics. Calnexin-deficient cells compensated for the loss of this function by partially shifting energy generation to the glycolytic pathway. These cells also showed closer apposition between the ER and mitochondria. Calnexin therefore controls the cellular energy balance between oxidative phosphorylation and glycolysis.**

## INTRODUCTION

Interorganellar contacts between the endoplasmic reticulum (ER) and mitochondria were first described in liver tissue recovering from prolonged nutrient deprivation (*1*–*3*). These ER-mitochondria contacts undergo dynamic changes and become most prominent immediately upon the removal of nutrition (*4*, *5*). These findings suggest a mechanistic link between these structures and the control of cellular metabolism (*6*). In mammalian cells, ER-mitochondria $Ca^{2+}$ signaling is central to this function (*7*). $Ca^{2+}$ signaling requires the tethering of the ER to mitochondria, often through multimeric protein complexes (*8*) such as the inositol 1,4,5-trisphosphate receptor ($IP_3R$)/voltage-dependent anion channel (VDAC) complex (*9*) or the ER-mitochondria encounter structure (ERMES). This multimeric protein complex (*8*) is represented in mammalian cells by the paralog of its Mmm1 component (*10*), the mammalian PDZ domain containing protein 8 (PDZD8) (*11*). However, the molecular machinery allowing ER-mitochondria contacts to react to metabolic and stress insults remains incompletely understood.

An intriguing, universal link exists between the enzymes that mediate oxidative protein folding and that control mitochondrial bioenergetics (*12*). Over the years, this link has been solidified through the discovery of numerous chaperones and folding assistants that cofractionate with mitochondria-associated membranes (MAMs) (*13*). These proteins include Ero1α (*14*) and ERp44 (*15*), two oxidoreductases that compete to bind to $IP_3Rs$. In addition, the chaperone calnexin and the disulfide isomerase TMX1 have been found in MAMs in unbiased proteome studies (*16*, *17*). Both calnexin (*18*) and TMX1 interact with sarco/endoplasmic reticulum $Ca^{2+}$ adenosine triphosphatase (ATPase) (SERCA) at MAMs (*19*). Through this interaction, TMX1 decreases ER $Ca^{2+}$ pumping, thus directing $Ca^{2+}$ flux toward mitochondria. In the absence of TMX1, mitochondria move closer to the plasma membrane to compensate for their $Ca^{2+}$ needs in the presence of hyperactive SERCA (*20*). Typically, however, SERCA activity positively aligns with mitochondrial metabolism, as shown by the activation of oxidative phosphorylation (OXPHOS) observed upon inhibition or knockdown of another SERCA inhibitor, Bcl-2 (*21*, *22*). Likewise, the knockout of the SERCA activator p53 results in increased sulfenylation of SERCA (*23*) but decreased mitochondrial OXPHOS (*24*, *25*). Although results from our laboratory have implicated the chaperone calnexin in the activation of SERCA (*18*), our data seemed to contradict an earlier study showing that overexpression of calnexin reduces cytosolic $Ca^{2+}$ waves (*26*), which is associated with reduced SERCA activity (*27*). In the present manuscript, we identified the mechanistic causes and consequences of these observations and demonstrated a critical role for calnexin in controlling mitochondrial positioning and metabolism.

## RESULTS

### Calnexin activates SERCA by maintaining its redox state

We previously proposed that calnexin activates SERCA (*18*), apparently contradicting previous observations that had been interpreted as calnexin acting as an inhibitor of SERCA (*26*). However, neither study took into account the complex interplay between ER and mitochondria $Ca^{2+}$ storage and buffering and membrane contact formation between the two organelles. SERCA activity is highest when luminal and cytosolic cysteines are partially oxidized (*28*, *29*). Although hyperoxidized SERCA is inactive, a baseline level of SERCA oxidation is necessary for its activity (*30*). Thus, we determined the SERCA2b redox state in calnexin wild-type and knockout mouse embryonic fibroblasts (MEFs) in the presence of a cysteine-recognizing biotinylated compound. We performed a biotinylated iodoacetamide (BIAM) switch assay on Myc immunoprecipitates from wild-type and knockout MEFs transfected with Myc-tagged SERCA2b (*31*, *32*). Under control conditions, SERCA2b was partially oxidized

[1]Faculty of Medicine and Dentistry, Department of Cell Biology, University of Alberta, Edmonton, Alberta T6G 2H7, Canada. [2]Complex Systems Research Center, Shanxi University, Taiyuan 030006, China. [3]Department of Anesthesiology and Pain Medicine, University of Alberta, Edmonton, Alberta T6G 2H7, Canada. [4]Department of Biochemistry and National Field Nuclear Magnetic Resonance Centre (Nanuc), University of Alberta, Edmonton, Alberta T6G 2H7, Canada. [5]Gottfried Schatz Research Center for Cell Signaling, Metabolism and Aging, Medical University of Graz, 8010 Graz, Austria. [6]Department of Physiology, University of Alberta, Edmonton, Alberta T6G 2H7, Canada. [7]Department of Physics, and State Key Laboratory of Cellular Stress Biology, Innovation Center for Cell Signaling Network, Xiamen University, Xiamen 361005, China.
*Corresponding author. Email: thomas.simmen@ualberta.ca

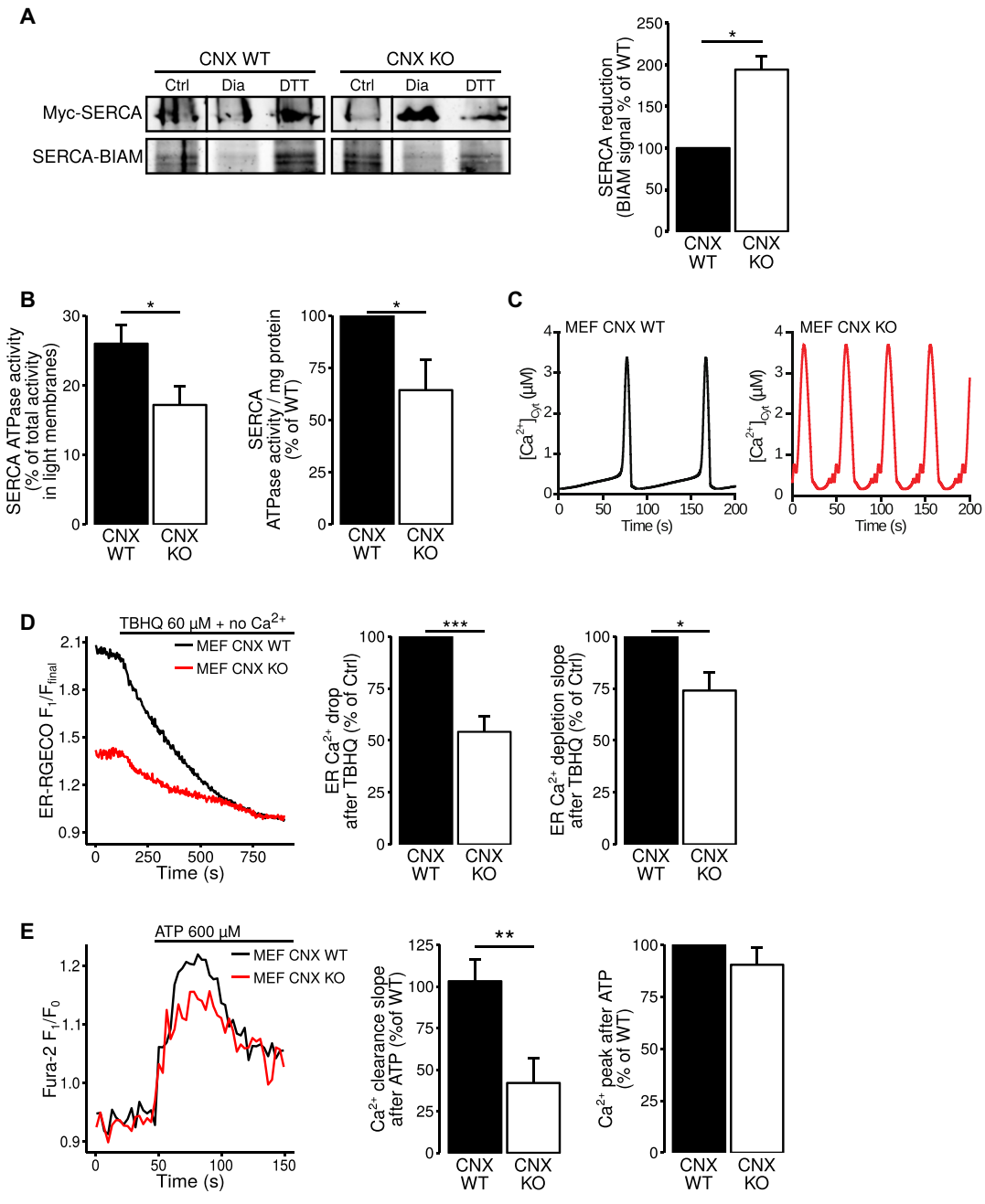


**Fig. 1. Calnexin activates SERCA by maintaining its redox state.** (**A**) Analysis of SERCA2b for the exposure of reduced cysteines, as detected with biotinylated iodoacetamide (BIAM). Cells were analyzed by Western blot for the Myc and BIAM signals. The BIAM signal from knockout MEFs was normalized to the signals from wild-type MEFs ($n = 4$ biological replicates for each group, $^*P = 0.001$ by one-sample $t$ test). (**B**) Light membranes were biochemically isolated from calnexin wild-type and knockout MEFs and cellular SERCA ATPase activity was determined in the presence of the SERCA inhibitor thapsigargin ($n = 7$ biological replicates for each group, $^*P = 0.04$ by two-sample $t$ test). SERCA ATPase activity was normalized to protein concentration in light membranes in calnexin wild-type and knockout MEFs ($n = 7$ biological replicates for each group, $^*P = 0.04$ by one-sample $t$ test). (**C**) Mathematical modeling of cytoplasmic $Ca^{2+}$ waves, taking into account activating calnexin modification of SERCA, as predicted in wild-type and calnexin knockout cells. (**D**) ER $Ca^{2+}$ was assayed upon tert-BuBHQ-mediated $Ca^{2+}$ release from the ER in wild-type and calnexin knockout MEFs transfected with ER-GECO. The drop of the fluorescent signal was recorded and average drops ($n = 12$ biological replicates for each group, $^{***}P = 0.000006$ by one-sample $t$ test) and depletion slopes ($n = 13$ biological replicates for each group, $^*P = 0.01$ by one-sample $t$ test) were quantified. (**E**) Cytoplasmic $Ca^{2+}$ was quantified by fluorimeter in wild-type and knockout MEFs loaded with Fura-2. ATP (600 μM) was added to open $IP_3Rs$ and induce $Ca^{2+}$ efflux from the ER, as indicated. Cytoplasmic $Ca^{2+}$ clearance was determined by the decay slope ($n = 6$ biological replicates for each group, $^{**}P = 0.002$ by one-sample $t$ test). The peak of cytoplasmic $Ca^{2+}$ was also determined ($n = 6$, $P = 0.31$ by one-sample $t$ test).

in wild-type MEFs, as determined from baseline signals established with dithiothreitol (DTT) and diamide treatment (Fig. 1A). In contrast, SERCA2b from calnexin knockout MEFs was fully reduced (Fig. 1A). Similarly, SERCA2b lost its partial oxidation in HeLa cells transfected with calnexin-directed small interfering RNA (siRNA) (siCNX) (fig. S1A). This finding suggested that calnexin was required to keep SERCA2b active. Consistent with this hypothesis, we detected a 35% reduction in SERCA-derived ATPase activity in cellular membranes from calnexin knockout MEFs as compared to those from wild-type MEFs (Fig. 1B). In siCNX-transfected HeLa cells, this reduction was not significant (fig. S1, B and C). In contrast, calnexin knockout cells stably reconstituted with wild-type calnexin (fig. S1, D and E) showed increased SERCA activity.

To determine the relevance of these findings to cytosolic $Ca^{2+}$ levels, we first used our mathematical $Ca^{2+}$ signaling model (*33*). We set the Hill function as activating to be consistent with our results suggesting that calnexin stimulated the ATPase activity of SERCA. We entered calnexin at a molarity of 0.05 and 0 μM into our model, corresponding to wild-type and knockout MEFs, respectively. Moreover, we also entered an ideal resting ER-mitochondria distance of 30 nm (*34*). The simulation results (Fig. 1C) showed that calnexin slowed down the frequency of cytosolic $Ca^{2+}$ waves by 56%, consistent

with published observations (*26*) leading to overall reduced availability of $Ca^{2+}$ in the cytoplasm. Running our mathematical model with an increased ER-mitochondria distance of 150% again showed that calnexin slowed down the frequency of cytosolic $Ca^{2+}$ waves by 32%, whereas entering calnexin as a SERCA inhibitor (by setting the Hill function as negative) had the opposite effect and further decreased cytosolic $Ca^{2+}$ waves (fig. S1F). To further test whether calnexin activated SERCA, we determined how calnexin affected $Ca^{2+}$ availability within the ER and the cytoplasm. We used the ER-targeted $Ca^{2+}$ probe ER-RGECO to measure the total amount of $Ca^{2+}$ in the ER in cells treated with the SERCA inhibitor tert-BuBHQ (TBHQ) and upon removal of extracellular $Ca^{2+}$ to completely deplete ER stores (Fig. 1D). In calnexin knockout MEFs, the ER-RGECO signal was reduced by 50% and the rate of the $Ca^{2+}$ drop was decreased, thus suggesting that these cells not only have less ER $Ca^{2+}$ content but also retain ER $Ca^{2+}$ better (Fig. 1D, right). Consistent with the ATPase results (fig. S1C), the ER $Ca^{2+}$ content did not differ substantially between control and siCNX-transfected HeLa cells (fig. S1G). In contrast, the reconstitution of calnexin knockout MEFs with wild-type calnexin partially restored ER $Ca^{2+}$ content (fig. S1H).

Use of the translocon inhibitor anisomycin abolished the difference in leak between wild-type and knockout MEFs, suggesting that calnexin promoted $Ca^{2+}$ leakage from the ER through the translocon (fig. S2A). The reduction in ER $Ca^{2+}$ in calnexin knockout MEFs could be due to decreased store-operated $Ca^{2+}$ entry (SOCE), which we tested by adding $Ca^{2+}$ to the medium of previously $Ca^{2+}$-starved cells while inhibiting SERCA. Calnexin knockout MEFs took up more $Ca^{2+}$ under this condition (fig. S2B), suggesting that calnexin may inhibit SOCE but ruling out decreased SOCE as an explanation for the reduced $Ca^{2+}$ content in calnexin knockout MEFs. Last, we measured the speed at which $Ca^{2+}$ was cleared from the cytosol after a controlled release of $Ca^{2+}$ through $IP_3R$ opening using the cytosolic $Ca^{2+}$ indicator dye Fura-2 (Fig. 1E). Calnexin knockout MEFs exhibited >50% reduction of the cytosolic $Ca^{2+}$ clearance speed compared to wild-type MEFs, corroborating reduced SERCA activity in the absence of calnexin (Fig. 1E, left). The amplitude of the $Ca^{2+}$ signal in the cytoplasm was unchanged (Fig. 1E, right). Together, our data showed that calnexin determines the ER $Ca^{2+}$ content predominantly by maintaining the SERCA redox state and increases SERCA-mediated $Ca^{2+}$ uptake from the cytoplasm. Within the cytoplasm, calnexin reduced the availability of $Ca^{2+}$ by increasing its clearance.

## Calnexin influences mitochondria positioning

The spatial arrangement of mitochondria depends on the amounts of cytosolic $Ca^{2+}$, which at high levels arrest mitochondria by blocking mitochondrial motor proteins (*35*, *36*), thus explaining why the ER-mitochondria distance depends on cytosolic $Ca^{2+}$ levels (*37*, *38*). Because calnexin knockout delayed $Ca^{2+}$ clearance, thus potentially increasing $Ca^{2+}$ levels in the proximity of the ER, we hypothesized that the absence of calnexin could reduce ER-mitochondria distance. We first modeled the effects of calnexin on ER-mitochondria distance based on the inhibitory effect of cytosolic $Ca^{2+}$ for mitochondria movement (*37*, *38*). In our model, we fixed $r_0$, the minimum distance derived from spatial constraints between the ER and the inner mitochondrial membrane (IMM) at a constant value in the range from 5 to 35 nm. Next, we set $r_c$ as the maximum modulatory distance of 35 nm. We then corrected $r_c$ to take into account the repelling force of low levels of $[Ca^{2+}]_{cyt}$ that are more frequent if waves are inhibited. This effect increases the actually expected distances ($r = r_0 + r_c$) to at least 25 to 30 nm (Fig. 2A). From published results (*26*) and our measurements and modeling (Fig. 1, C and D), we expected $r_c$ to be lower in calnexin knockout cells, leading to reduced distance in this case. At an $r_0$ of 20 nm, which is close to the minimum physically possible ER-IMM distance (*34*), the predicted effective distance $r$ was 29 nm for calnexin knockout MEFs and 42 nm for wild-type MEFs (Fig. 2A). This 31% decrease in the distance between ER and mitochondria in calnexin knockout MEFs would be consistent with the 50% slower $Ca^{2+}$ clearance in calnexin knockout MEFs (Fig. 1D) that would be expected to increase cytosolic $Ca^{2+}$ puffs and oscillations (Fig. 1C).

Next, to corroborate these in silico results in cells, we determined the ER-mitochondria average distance in calnexin wild-type and knockout MEFs on electron micrographs (Fig. 2B). The observed average distance between the ER and the outer mitochondrial membrane was 20 nm in calnexin knockout MEFs and 26 nm in calnexin wild-type MEFs, or about 30% wider (Fig. 2C), which correlated well with the predictions of our mathematical model. Moreover, we also detected increased mitochondria-ER contact (MERC) length in calnexin knockout MEFs (Fig. 2D), which led to an overall significantly increased MAM coefficient in calnexin knockout MEFs over calnexin wild-type MEFs (Fig. 2E). The analysis of the frequency of the different MERC types, classified as super tight (0 to 12 nm), tight (12 to 24 nm), and loose (24 to 50 nm), showed that the absence of calnexin promoted an increase in the frequency of super tight MERCs and a reduction in that of loose MERCs (Fig. 2F). We also analyzed calnexin knockout MEFs with a split-green fluorescent protein–based contact site sensor (SPLICS) system that can quantify tight ($SPLICS_{short}$) and loose contacts ($SPLICS_{long}$) but not super-tight MERCs (*39*). This system showed no difference in tight MERCs (Fig. 2G), but in contrast to our electron micrograph analysis, we found more signals for loose MERCs in calnexin knockout MEFs (Fig. 2H). This slightly different result could derive from the larger sample size of the SPLICS assay. Together, our results demonstrate in silico and in cells that the activation of SERCA by calnexin controlled $Ca^{2+}$ clearance on the cytosolic face of the ER and apposition between the ER and mitochondria.

## Calnexin controls mitochondrial $Ca^{2+}$ responses

Our results so far indicated that calnexin increased ER $Ca^{2+}$ content, cytosolic $Ca^{2+}$ clearance, and ER-mitochondria apposition. Each of these properties might alter availability of $Ca^{2+}$ at mitochondria, but the final mitochondrial $Ca^{2+}$ and membrane potential readouts might depend on the combination of effects or the effects might cancel each other out. To distinguish between these two possibilities, we used the sensitive mitochondria-targeted $Ca^{2+}$ probe mito-RGECO, which allows a wider detection range of $Ca^{2+}$ spikes in mitochondria than the high-affinity Rhod2 probe (*40*). $IP_3R$-mediated $Ca^{2+}$ release from the ER and uptake into mitochondria did not result in significantly increased $Ca^{2+}$ transfer in either cell type (fig. S2C). However, application of the protonophore carbonyl cyanide *p*-trifluoromethoxyphenylhydrazone (FCCP) revealed that the mitochondrial free $Ca^{2+}$ content was 25% higher in wild-type MEFs than in calnexin knockout MEFs (Fig. 3A). This free mitochondrial $Ca^{2+}$ content decreased to a greater extent upon removal of extracellular $Ca^{2+}$ in calnexin wild-type MEFs compared with knockout MEFs (Fig. 3B), suggesting that calnexin is important to retain $Ca^{2+}$ not just within the ER (Fig. 1D) but also within mitochondria of wild-type MEFs.

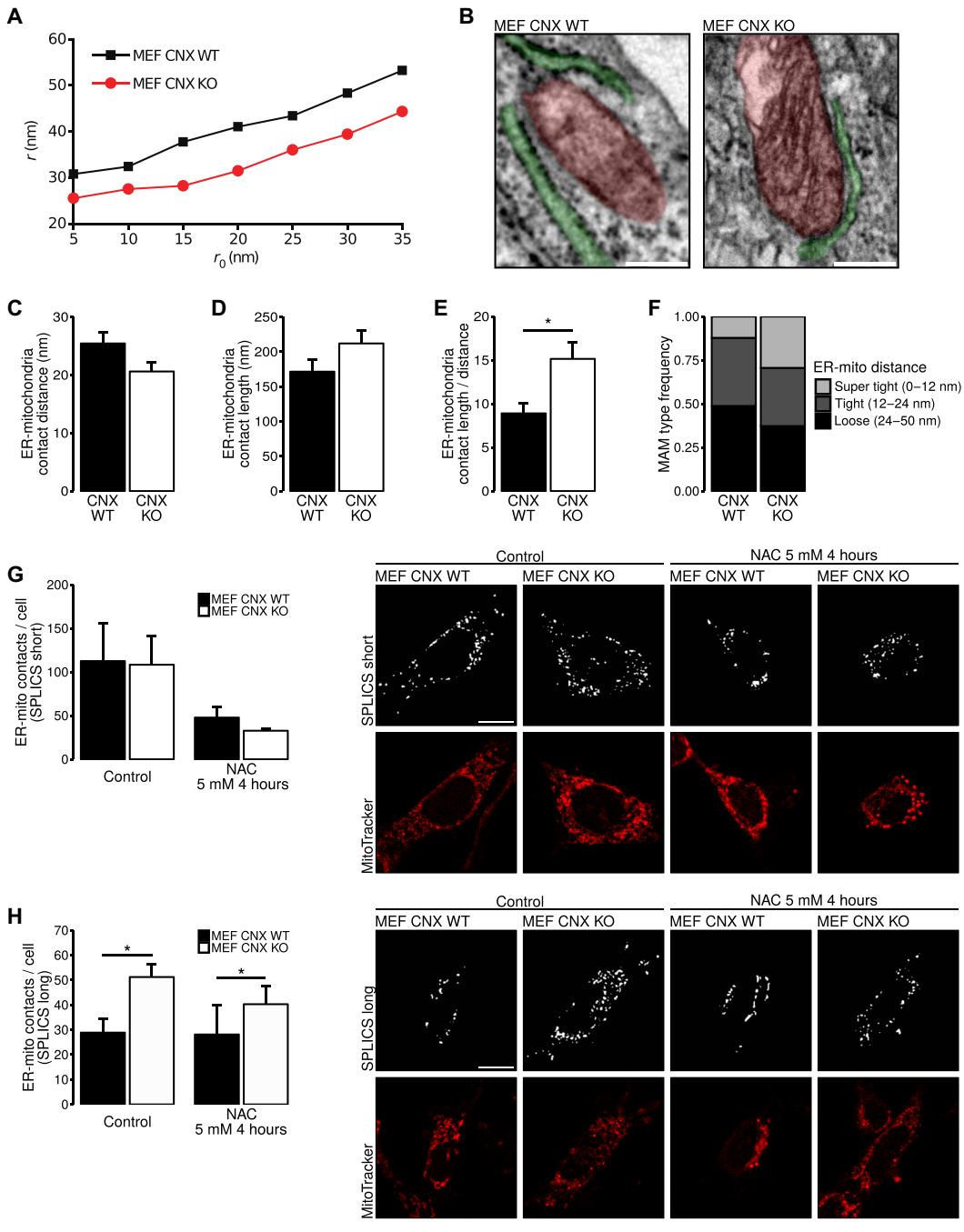


**Fig. 2. Slower cytosolic clearance is associated with closer MERCs in calnexin knockout cells.** (**A**) Mathematical modeling of ER-mitochondria distance, taking into account calnexin expression (WT = 0.05 μM calnexin; KO = no calnexin). Depending on $r_0$, the minimum distance between the two organelles, $r_c$ was determined as a function of cytosolic [$Ca^{2+}$]. *r* corresponds to the sum of the two and is the postulated actual distance between the ER and mitochondria. (**B**) Representative electron microscopy images of calnexin wild-type and knockout MEFs. Mitochondria are labeled in red and ER is labeled in green. Scale bar, 200 nm. (**C**) Average ER-mitochondria distance as determined from electron micrographs ($P = 0.07$ by two-sample Wilcoxon test; $n = 41$ MERCs for wild-type MEFs, $n = 51$ MERCs for knockout MEFs). (**D**) Average ER-mitochondria contact length as determined from electron micrographs ($P = 0.15$ by two-sample Wilcoxon test; $n = 41$ MERCs for wild-type MEFs, $n = 51$ MERCs for knockout MEFs). (**E**) Coefficient of ER-mitochondria contact length divided by ER-mitochondria distance (*$P = 0.03$ by two-sample Wilcoxon test; $n = 41$ MERCs for wild-type MEFs, $n = 51$ MERCs for knockout MEFs). (**F**) Split of distance-sorted ER-mitochondria contacts into super-tight contacts (<12 nm), tight contacts (12 to 24 nm), and loose contacts (24 to 50 nm), derived from (B) to (E). (**G**) $SPLICS_{short}$ signals were determined by quantifying signal dots per cell (Control: MEF CNX WT $n = 11$ cells, MEF CNX KO $n = 23$ cells, $P = 0.81$ by two-sample Wilcoxon test; NAC: MEF CNX WT $n = 9$ cells, MEF CNX KO $n = 19$ cells, $P = 0.26$ by two-sample Wilcoxon test). Scale bar, 20 μm. (**H**) $SPLICS_{long}$ signals were determined by quantifying signal dots per cell (Control: MEF CNX WT $n = 8$ cells, MEF CNX KO $n = 9$ cells, *$P = 0.01$ by two-sample Wilcoxon test; NAC: MEF CNX WT $n = 8$ cells, MEF CNX KO $n = 10$ cells, *$P = 0.04$ by two-sample Wilcoxon test). Scale bar, 20 μm.

To further investigate a potential role of calnexin for mitochondria, we next assayed the $Ca^{2+}$ responsiveness of the mitochondrial membrane potential ($\Delta\Psi$) to $Ca^{2+}$. Although $\Delta\Psi$ did not substantially differ between calnexin wild-type and knockout MEFs (Fig. 3C), its responsiveness to artificial, thapsigargin-triggered ER-mitochondria $Ca^{2+}$ flux was increased threefold in calnexin knockout MEFs (Fig. 3D). Together, these results indicated that mitochondria in calnexin knockout MEFs were depleted of $Ca^{2+}$. Potentially as an adaptation, they were more responsive to ER-derived $Ca^{2+}$ if pharmacologically provided with it.

## Calnexin regulates mitochondria metabolism

Our results indicated that calnexin could activate mitochondria (because of the increase in mitochondria $Ca^{2+}$ content; Fig. 3, A and B) or inhibit them (because of the increased ER-mitochondria distance; Fig. 2, E and H) or the two effects might cancel each other out (as seen with the $IP_3R$-mediated $Ca^{2+}$ transfer to mitochondria; fig. S1C). We sought to distinguish between these possibilities. First, we measured total cellular adenosine 5′-triphosphate (ATP) levels, which showed a small reduction in calnexin knockout MEFs (Fig. 4A). However, this value is derived from a combination of

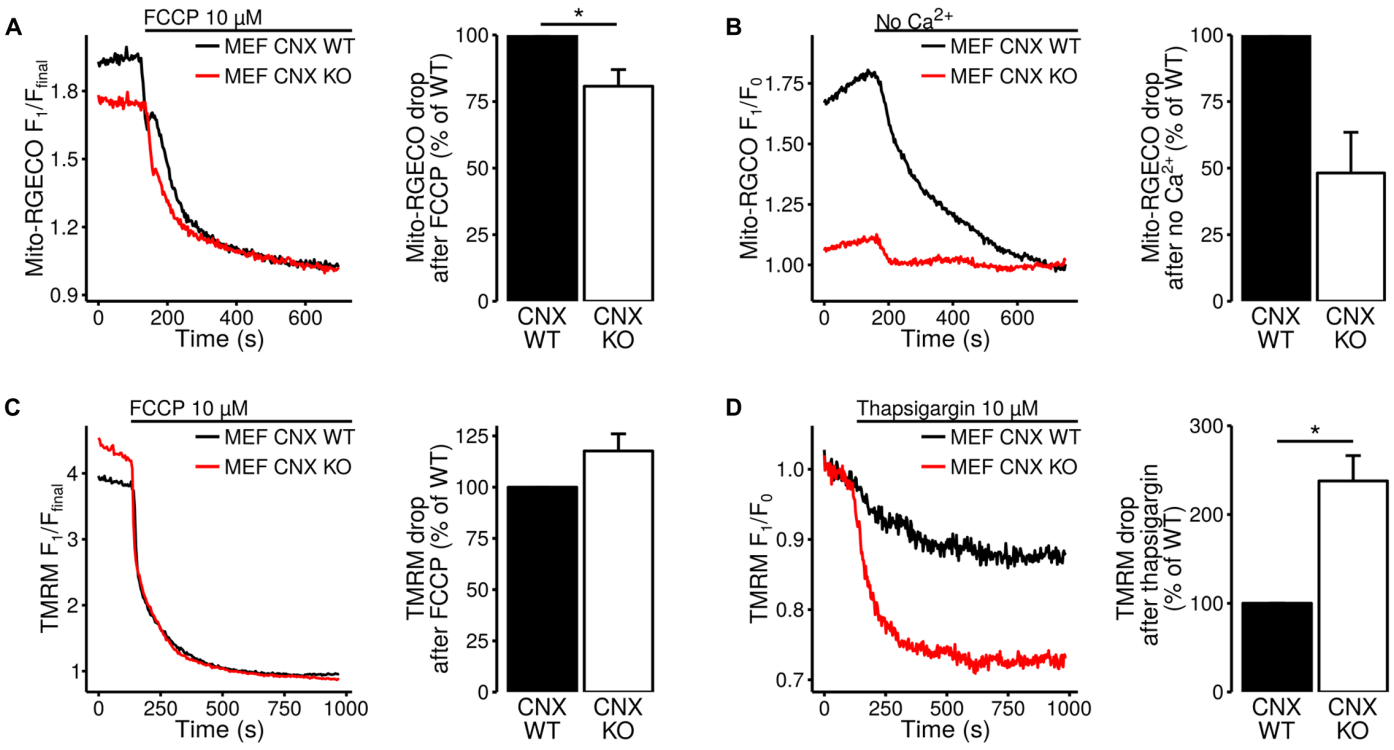


**Fig. 3. $Ca^{2+}$-deprived mitochondria are more responsive to artificially ER-released $Ca^{2+}$ in calnexin knockout cells.** (**A**) Wild-type and calnexin knockout MEFs were transfected with Mito-GECO and imaged by fluorescence microscopy to measure total mitochondrial $Ca^{2+}$. As indicated, 10 μM FCCP was added to disable mitochondrial $Ca^{2+}$ transport ($n = 4$ biological replicates for each group, $^*P = 0.05$ by one-sample $t$ test). (**B**) Wild-type and calnexin knockout MEFs were transfected with Mito-GECO. As indicated, $Ca^{2+}$ was removed from the growth medium and cells were imaged by fluorescence microscopy to measure total mitochondrial $Ca^{2+}$ ($n = 3$ biological replicates for each group, $P = 0.07$ by one-sample $t$ test). (**C**) Wild-type and calnexin knockout MEFs were loaded for 30 min with 40 nM TMRM. Mitochondrial potential was measured and, as indicated, 10 μM FCCP was added to uncouple mitochondria. The average FCCP-induced decrease in the TMRM fluorescent signal was quantified ($n = 3$ biological replicates for each group, $^*P = 0.17$ by one-sample $t$ test). (**D**) Wild-type and calnexin knockout MEFs were loaded with TMRM as in (C). Mitochondrial potential was measured and, as indicated, 10 μM thapsigargin was added to release $Ca^{2+}$ from the ER. The average thapsigargin-induced decrease in the TMRM fluorescent signal was quantified ($n = 3$ biological replicates for each group, $^*P = 0.04$ by one-sample $t$ test).

mitochondrial and glycolytic energy production. We therefore tested whether there was a connection between calnexin and OXPHOS or glycolysis. We found that wild-type MEFs, but not calnexin knockout MEFs, showed a robust reduction in ATP upon oligomycin treatment (Fig. 4B). In contrast, 2-deoxyglucose affected both wild-type and calnexin knockout MEFs to a similar extent (Fig. 4B). Because oligomycin blocks OXPHOS, but 2-deoxyglucose interferes with both OXPHOS and glycolysis (*41*), our results suggested that calnexin deficiency still allowed for respiration but led to a greater relative reliance on glycolysis. Overall, these data suggest that calnexin maintains normal OXPHOS.

We also measured the abundance of select proteins that control glycolysis. There was a 50% increase in the amount of hexokinase 1 in calnexin knockout MEFs, consistent with increased levels of glycolysis in calnexin knockout cells (Fig. 4C). In contrast, we did not detect differing amounts of mitochondrial proteins between genotypes (Fig. 4C). Likewise, we did not detect differences in mitochondria mass, number, or size (Fig. 4D). In contrast, intact calnexin knockout MEFs showed reduced basal respiration resulting in a 45% reduction in electron transport chain capacity compared to wild-type cells upon normalization to citrate synthase activity (Fig. 4E). This phenotype was reproduced in HeLa cells transfected with calnexin RNA interference (RNAi) compared to cells transfected with scramble RNAi (fig. S2D). Mitochondrial enzymatic activity measurements showed a 38% increase in citrate synthase activity in calnexin knockout MEFs under experimental conditions that supplied mitochondria with external $Ca^{2+}$ (Fig. 4F). This phenotype prompted us to measure intramitochondrial ATP levels. Although mitochondria in calnexin knockout MEFs did not have different baseline ATP levels, these mitochondria had a threefold increased ability to rescue their ATP content upon an OXPHOS block (Fig. 4G). We also measured glucose consumption and lactate secretion of calnexin wild-type and knockout MEFs, which showed that calnexin deficiency did not significantly alter the glycolytic flux (fig. S2E). This metabolic signature indicated that calnexin knockout MEFs can compensate for the decrease in OXPHOS-derived energy generation with increased glycolysis and improved Krebs cycle capacity.

To analyze the importance of these findings, we measured the activity of the key metabolic sensor adenosine 5′-monophosphate–activated protein kinase (AMPK). Consistent with their altered energy balance, calnexin knockout MEFs showed a 50% increased activity of AMPK (Fig. 4H). Last, we hypothesized that blocking OXPHOS would be less toxic to calnexin knockout MEFs because they rely more on glycolysis than OXPHOS. Treatment with oligomycin and rotenone induced apoptosis to a lesser extent in calnexin knockout MEFs, confirming a reduced reliance on mitochondrial OXPHOS in these cells (Fig. 4I). Together, our results demonstrated that the role of the ER chaperone calnexin in mitochondrial bioenergetics is to maintain mitochondrial OXPHOS. In the absence

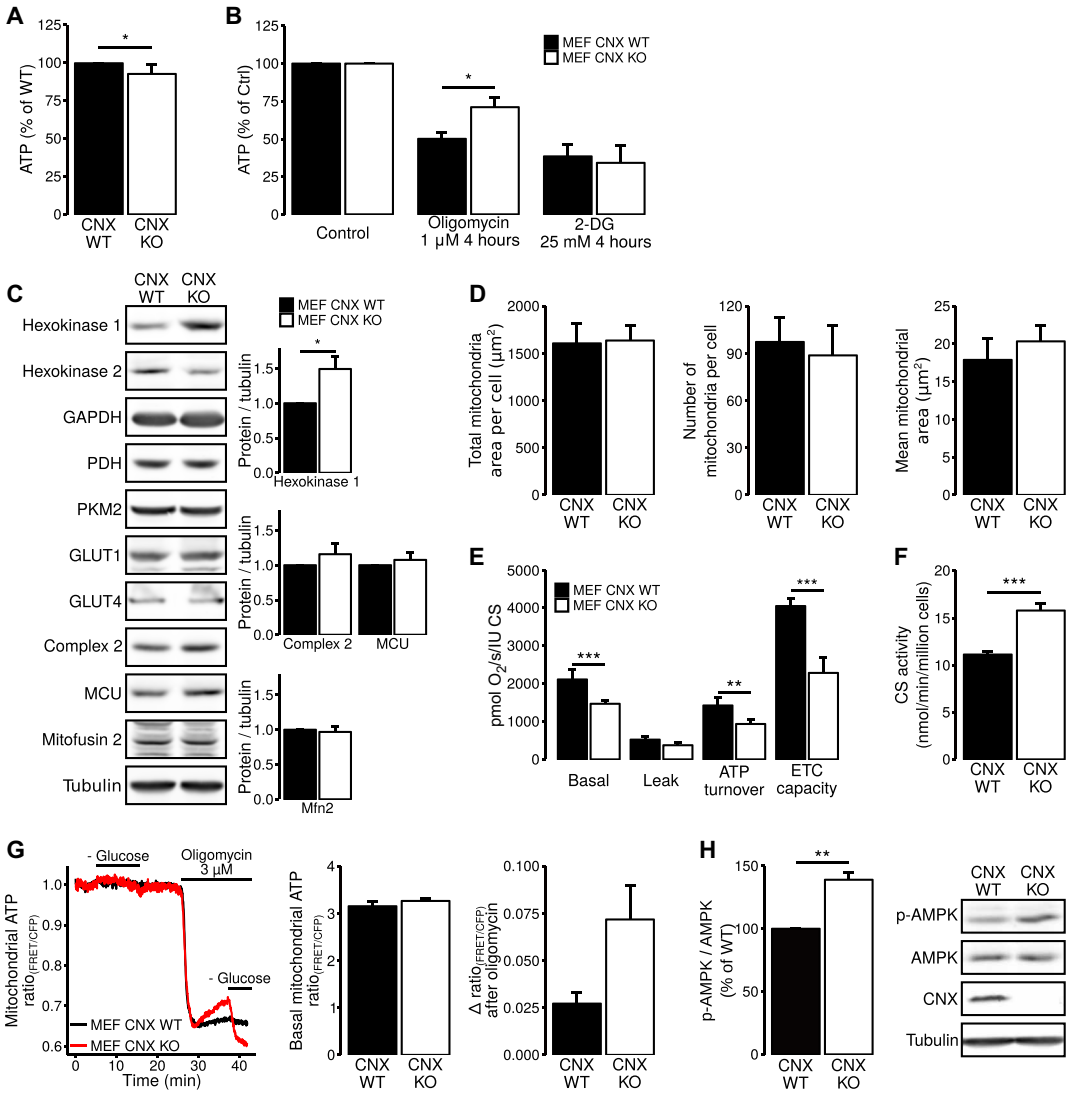


**Fig. 4. Calnexin allows for normal mitochondria metabolism.** (**A**) Total cellular ATP content was measured in wild-type and calnexin knockout MEFs ($n = 35$ biological replicates for each group, $^*P = 0.04$ by two-sample Wilcoxon test). (**B**) After incubation with 1 μM oligomycin for 4 hours (in high glucose DMEM) or with 25 mM 2-deoxyglucose (2-DG, in DMEM lacking glucose) for 4 hours, total ATP content was measured in wild-type and calnexin knockout MEFs (oligomycin $n = 6$ sets of cells for each group, $^*P = 0.02$ by two-sample $t$ test; 2-DG $n = 4$ sets of cells for each group, $P = 0.34$ by two-sample Wilcoxon test). (**C**) Calnexin wild-type and knockout MEFs were immunoblotted for the indicated glycolytic and mitochondrial proteins. Hexokinase 1 ($n = 5$ sets of cells for each group, $^*P = 0.04$ by one-sample $t$ test), mitochondrial complex 2 ($n = 3$ sets of cells for each group, $P = 0.5$ by two-sample Wilcoxon test), MCU ($n = 8$ sets of cells for each group, $P = 0.4$ by two-sample Wilcoxon test), and mitofusin-2 ($n = 3$ sets of cells for each group, $P = 0.7$ by one-sample $t$ test). $n \geq 2$ sets of cells for all other proteins. (**D**) Wild-type and calnexin knockout MEFs were loaded with 1 μM Mitotracker Green for 30 min and assayed for the total mitochondrial area per cell ($P = 0.9$ by two-sample $t$ test with equal variance), for the number of mitochondria ($P = 0.7$ by two-sample $t$ test with equal variance), and for the mean area of individual mitochondrial particles ($P = 0.5$ by two-sample $t$ test with equal variance). $n = 5$ sets of cells for wild type and $n = 6$ sets of cells for calnexin knockout MEFs. (**E**) Measurement of the mitochondrial oxygen consumption rates in wild-type and calnexin knockout MEFs. Basal respiration, leak, ATP turnover, and ETC capacity (pmol $O_2$/s/CS activity) were determined and plotted ($n = 10$ sets of cells for each group, $P = 0.0007$ by two-sample Wilcoxon test for Basal, $P = 0.06$ by two-sample Wilcoxon test for Leak, $^{***}P = 0.009$ by two-sample Wilcoxon test for ATP turnover, and $^{***}P = 0.00001$ by two-sample Wilcoxon test for ETC capacity). (**F**) Quantification of citrate synthase activity in wild-type and calnexin knockout MEFs ($n = 10$ sets of cells for each group, $^{***}P = 0.00001$ by two-sample Wilcoxon test). (**G**) Mitochondrial ATP within wild-type and calnexin knockout MEF cells were assessed using mtAT1.03 signals. Quantification shown on the right (basal mitochondrial ATP: $n = 10$ sets of cells for each group, $P = 0.3$ by two-sample $t$ test with equal variance. Δ ratio: $n = 11$ set of cells, $P = 0.05$ by two-sample Wilcoxon test). (**H**) Analysis of protein lysates for AMPK activity, as assessed by the phospho-AMPK signal. Tubulin was used as a loading control ($n = 4$ sets of cells for each group, $^{**}P = 0.006$ by one-sample $t$ test). (**I**) Quantification of apoptosis as assessed by Annexin V and PI in calnexin wild-type and knockout MEFs incubated for 24 hours with oligomycin (1 μM) or rotenone (1 μM) (Control $n = 3$ sets of cells for each group, $P = 0.07$ by two-sample Wilcoxon test; oligomycin $n = 3$ sets of cells for each group, $^{**}P = 0.005$ by two-sample Wilcoxon test; rotenone $n = 3$ sets of cells for each group, $P = 0.07$ by two-sample Wilcoxon test).

of calnexin, cells compensate by increasing Krebs cycle capacity and glycolysis while becoming less vulnerable to OXPHOS disruption.

### Cells adapt to the absence of calnexin by boosting $Ca^{2+}$ flux across MAMs

We next examined whether calnexin knockout also altered MAM composition and function. First, we measured the expression of select MAM-regulatory proteins, focusing specifically on $IP_3R1$ and VDAC1, which control $Ca^{2+}$ flux from the ER to mitochondria. Calnexin knockout MEFs expressed about 50% more $IP_3R1$ and VDAC1 (Fig. 5A), reflecting their maintained ability to accept ER $Ca^{2+}$ signals from the ER, despite depleted ER $Ca^{2+}$ stores (fig. S2C), and consistent with their increased ER-mitochondria apposition. In contrast, the abundance of the ER proteins protein kinase RNA-like ER kinase (PERK), SERCA2b, ERp57, and Nox4 and the autophagy adaptor p62 did not differ between genotypes (Fig. 5A). However, an acute knockdown of calnexin led to small decreases in the amounts of SERCA2b and Nox4 (fig. S3A). Similarly, MAMs of calnexin knockout MEFs had a relatively small increase of the mitofusin-2 tether but otherwise did not show substantial changes (fig. S3B), suggesting that MAM composition was not affected in a major way by the absence of calnexin.

To further investigate the basis of the altered metabolism of calnexin knockout MEFs, we examined whether these cells relied on altered $Ca^{2+}$ handling. Chelation of intracellular $Ca^{2+}$ by 1,2-Bis(2-aminophenoxy)ethane-N,N,N′,N′-tetraacetic acid tetrakis(acetoxymethyl ester) (BAPTA)–AM reduced basal oxygen consumption rate (OCR) in wild-type cells by more than 50%, but only by about 35% in knockout MEFs (Fig. 5B), thus eliminating the significant difference between the OCRs of the two cell lines (Fig. 4E). This result suggests that the key metabolic differences in calnexin knockout MEFs stem from altered $Ca^{2+}$ flux at the MAM originating from a reduction of both ER $Ca^{2+}$ stores and SERCA activity.

### Oxidizing conditions are necessary for the metabolic roles of calnexin

Changes in SERCA activity could be due to different protein amounts or different activity. Our findings so far indicated that calnexin knockout or knockdown decreased redox-dependent posttranslational SERCA2b modifications that determine its activity to a greater extent (Fig. 1A and fig. S1A) than its total abundance (Fig. 5A and fig. S3A). We therefore sought to identify the source of SERCA2b-modifying reactive oxygen species (ROS). Calnexin knockout MEFs had lower cytosolic ROS as previously published (*42*) (Fig. 6A), but similar amounts of mitochondrial ROS to wild-type MEFs (Fig. 6A). Therefore, we surmised that ROS from outside the mitochondria trigger activating SERCA2b oxidation.

Thus, we sought to pharmacologically equalize the cytosolic redox status between the two cell types. Treatment with *N*-acetylcysteine (NAC), which does not affect the unfolded protein response (*43*, *44*), resulted in fully reduced SERCA2b in cells of both genotypes (Fig. 6B), as expected. Analysis of ER $Ca^{2+}$ loading through SERCA showed that NAC reduced ER $Ca^{2+}$ content and $Ca^{2+}$ release in calnexin wild-type MEFs, but not knockout MEFs (Fig. 6, C and D), thus indicating that NAC eliminated the $Ca^{2+}$ storage difference between the two genotypes. Consistent with this finding and with the role of ER $Ca^{2+}$ filling for mitochondrial OXPHOS, calnexin wild-type MEFs, but not knockout MEFs, exhibited markedly reduced respiration upon incubation with NAC (Fig. 6E), similar to treatment with BAPTA-AM (Fig. 5B). During the relatively short time frame of 4 hours, NAC did not correct the differences in the activity of the Krebs cycle enzyme citrate synthase (Fig. 6F). Similarly, NAC reduced basal OCR more in control HeLa cells, than in siCNX-transfected cells, and did not correct citrate synthase activity (fig. S4, A and B). Last, NAC also reduced the difference in the $SPLICS_{long}$ signal without affecting the $SPLICS_{short}$ signal in calnexin wild-type and knockout MEFs (Fig. 2, G and H).

Next, we sought to investigate the source of oxidative stress in wild-type MEFs by using inhibitors for two ER ROS producers, Ero1 (EN460) and Nox1/4 (GKT137831) (*45*, *46*). Both EN460 and GKT137831 decreased the SERCA2b oxidation state (fig. S5A) and partially reduced the ATPase activity of SERCA2b in wild-type MEFs, thus decreasing the difference in ATPase activity (fig. S5B) and ER $Ca^{2+}$ content (fig. S5C) between wild-type and knockout MEFs. These results suggested that a combined ER-derived ROS source was responsible for the correct SERCA2b redox and activity

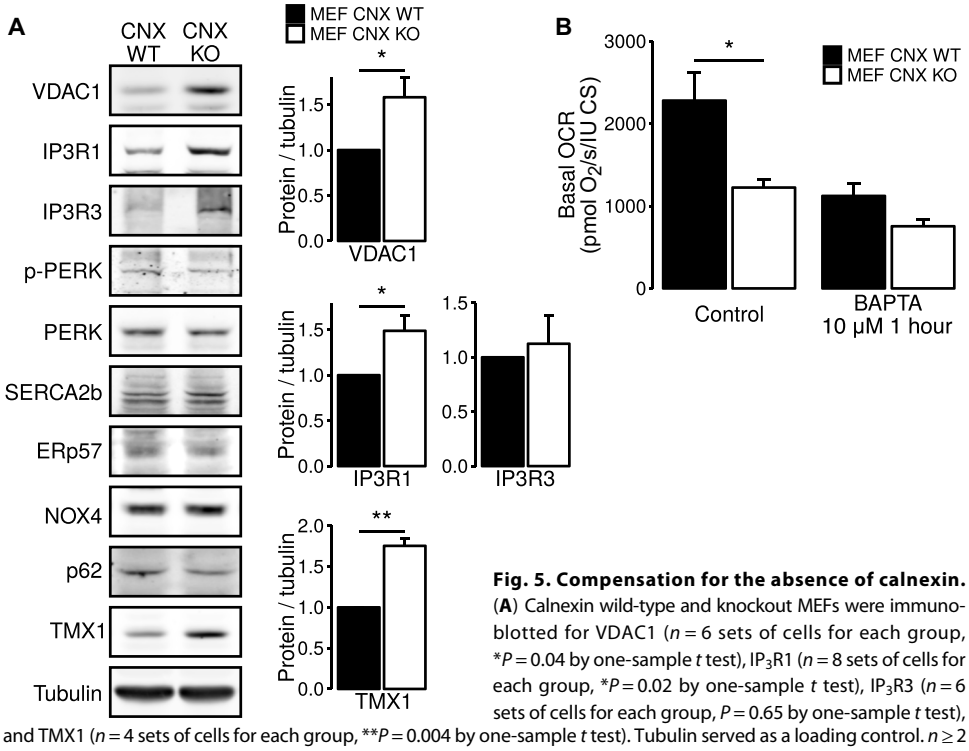


**Fig. 5. Compensation for the absence of calnexin.** (**A**) Calnexin wild-type and knockout MEFs were immunoblotted for VDAC1 ($n = 6$ sets of cells for each group, $^*P = 0.04$ by one-sample *t* test), $IP_3R1$ ($n = 8$ sets of cells for each group, $^*P = 0.02$ by one-sample *t* test), $IP_3R3$ ($n = 6$ sets of cells for each group, $P = 0.65$ by one-sample *t* test), and TMX1 ($n = 4$ sets of cells for each group, $^{**}P = 0.004$ by one-sample *t* test). Tubulin served as a loading control. $n \geq 2$ sets of cells for all other proteins. (**B**) Measurement of the basal mitochondrial oxygen consumption rates in wild-type and calnexin knockout MEFs upon incubation with 10 μM BAPTA-AM for 1 hour (Control $n = 5$ sets of cells for each group, $^*P = 0.02$ by two-sample *t* test with equal variance; BAPTA $n = 5$ sets of cells for each group, $P = 0.07$ by two-sample *t* test with equal variance).

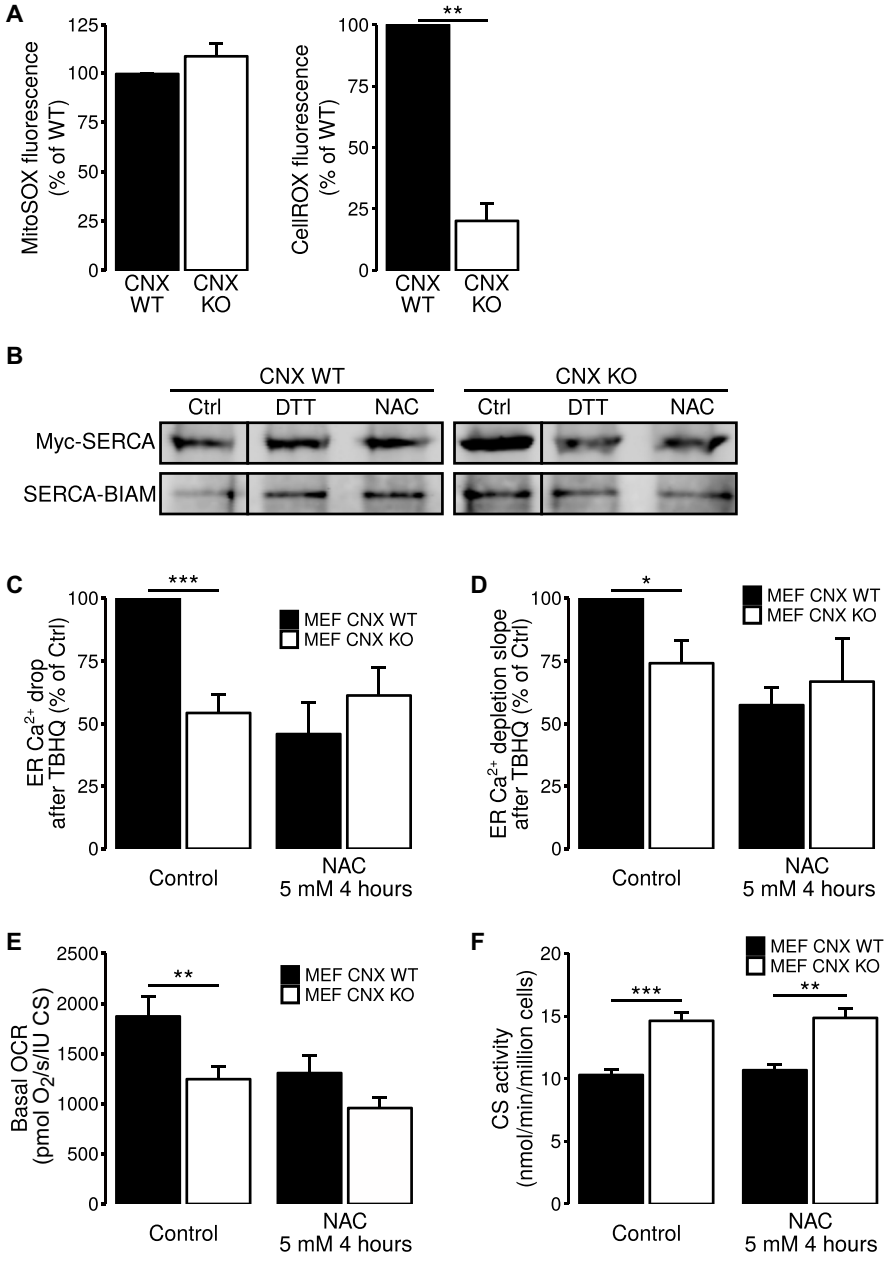


**Fig. 6. Equalization of SERCA2b redox state with NAC abolishes the different ER $Ca^{2+}$ and OXPHOS readouts between calnexin wild-type and knockout MEFs.** (**A**) Measurement of the cellular ROS production with flow cytometry to detect MitoSox (left) and CellROX (right) in wild-type and calnexin knockout MEFs ($n = 7$ sets of cells for each group, $P = 0.2$ by one-sample $t$ test for MitoSOX, $n = 3$ sets of cells for each group, $^{**}P = 0.008$ by one-sample $t$ test for CellROX). (**B**) Analysis of SERCA2b for the exposure of reduced cysteines, as detected with BIAM, in the presence of 5 mM NAC for 4 hours. Cells were analyzed by Western blot for Myc and BIAM signals. DTT-treated signals represent fully reduced SERCA2b ($n = 2$ independent experiments). (**C**) ER $Ca^{2+}$ measurements upon tert-BuBHQ-mediated $Ca^{2+}$ release from the ER in wild-type and calnexin knockout MEFs in the presence of 5 mM NAC for 4 hours ($n = 12$ biological replicates for each group, $^{***}P = 0.000005$ by one-sample $t$ test for Control; $n = 6$ biological replicates for each group, $P = 0.4$ by two-sample $t$ test with equal variance for NAC). (**D**) ER $Ca^{2+}$ depletion slope upon tert-BuBHQ-mediated $Ca^{2+}$ release from the ER in wild-type and calnexin knockout MEFs in the presence of 5 mM NAC for 4 hours ($n = 13$ biological replicates for each group, $^{*}P = 0.01$ by one-sample $t$ test for Control; $n = 6$ biological replicates for each group, $P = 0.6$ by two-sample $t$ test with equal variance for NAC). (**E**) Measurement of the basal mitochondrial oxygen consumption rates in wild-type and calnexin knockout MEFs upon incubation with 5 mM NAC for 4 hours ($n = 10$ biological replicates for each group, $^{**}P = 0.005$ by two-sample Wilcoxon test for Control, $P = 0.1$ by two-sample $t$ test with equal variance for NAC). (**F**) Quantification of citrate synthase activity in wild-type and calnexin knockout MEFs ($n = 10$ biological replicates for each group, $^{***}P = 0.000001$ by two-sample Wilcoxon test for Control; $n = 5$, $^{**}P = 0.001$ by two-sample $t$ test with equal variance for NAC).

and that the role of calnexin for mitochondrial $Ca^{2+}$ and metabolism is not connected to its role as a chaperone. Rather, our results suggest that calnexin maintains ER $Ca^{2+}$ levels and mitochondria metabolism by maintaining properly oxidized SERCA.

## DISCUSSION

An important function of MAMs is to establish a dedicated gateway for $Ca^{2+}$ between the ER and mitochondria (*47*). ER-derived $Ca^{2+}$ controls the activity of mitochondrial dehydrogenases (*48*) and hence the progression of the Krebs cycle (*49*). The flux of $Ca^{2+}$ ions between the ER and mitochondria controls mitochondrial metabolism, as shown by its disruption in cells lacking all versions of $IP_3R$, whose respiration is about one-third of their wild-type counterparts (*50*). Accordingly, these cells also activate signaling through AMPK (*50*). Understanding the proteins that control ER-mitochondria $Ca^{2+}$ transfer is therefore expected to yield insight into the control of cellular metabolism. Proteomic studies have identified ER chaperones and folding assistants as prominent MAM proteins (*16*, *17*). However, few mechanistic connections between ER chaperones, including calnexin, and mitochondrial respiration have been made.

Calnexin localizes in close proximity to the translocon, where it regulates protein folding (*51*), but it is also found on MAMs and is part of the SERCA2b interactome (*18*, *26*). Because the inhibition of SERCA decreases the $IP_3R$-mediated transfer of $Ca^{2+}$ to mitochondria (*52*), we hypothesized that by controlling SERCA activity, calnexin controls the flux of $Ca^{2+}$ between the ER and mitochondria and thus should have metabolic functions (Fig. 7). Calnexin knockout MEFs show about 30% less respiration, based on a reduction of SERCA cysteine oxidation by 54% (Fig. 1A) that led to a reduction of the SERCA activity by 32%, characteristics that were reproduced in HeLa cells transfected with calnexin RNAi and attenuated upon calnexin reconstitution. As an adaptation, calnexin knockout MEFs showed increased AMPK activation and increased MAMs, which coincided with an increased ability to use glucose within mitochondria upon OXPHOS inhibition (Fig. 4, G to I).

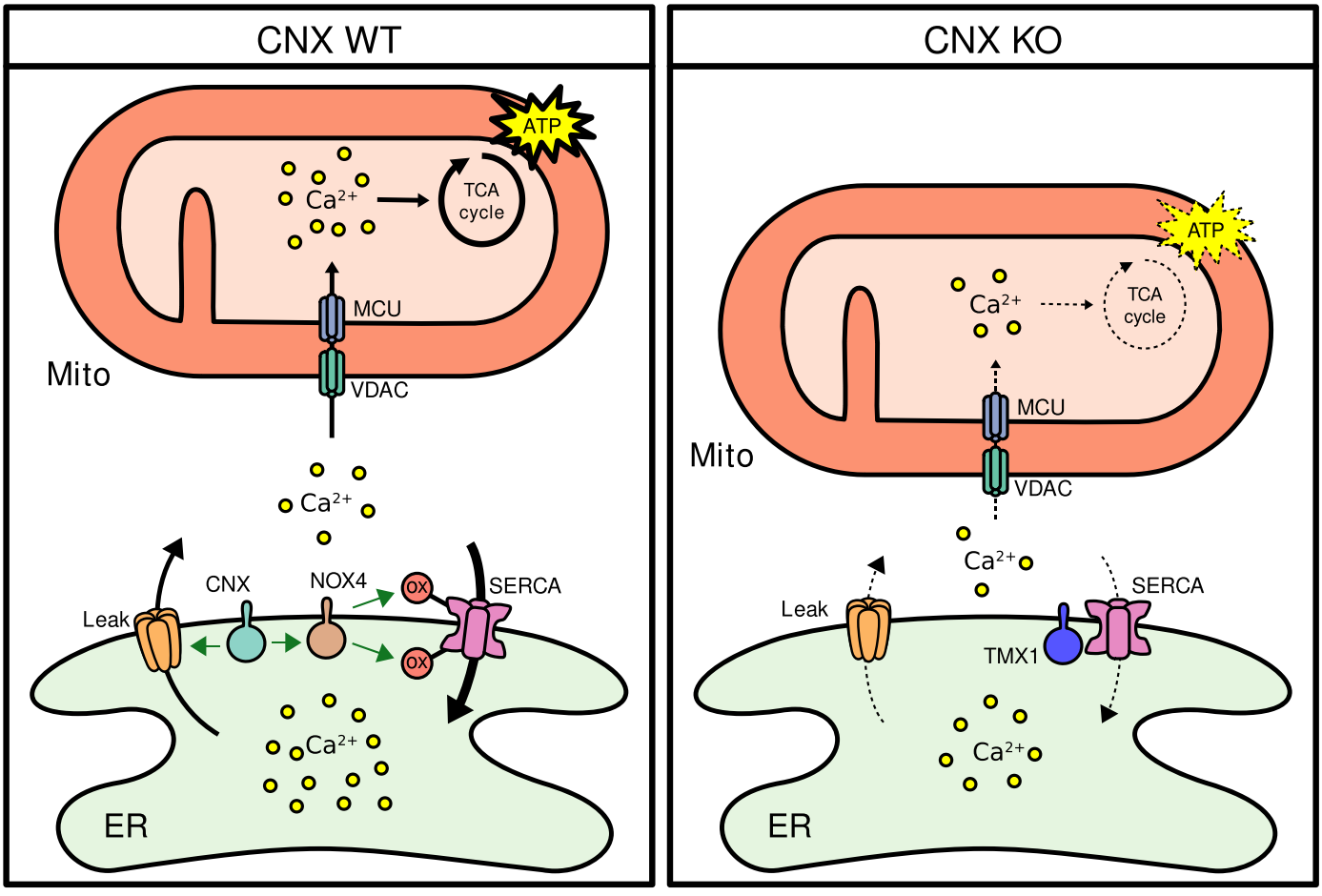


**Fig. 7. Summary of the role of calnexin for ER-mitochondria $Ca^{2+}$ flux and mitochondria metabolism.** The calnexin-mediated activation of SERCA through the maintenance of its redox state by Nox4 and other ER ROS sources allows for proper $Ca^{2+}$ filling of the ER. A properly filled ER is necessary to provide mitochondria with sufficient $Ca^{2+}$ necessary for the Krebs cycle and OXPHOS. In the absence of calnexin, cells compensate for the reduced $Ca^{2+}$ flux with closer ER-mitochondria apposition. This compensation is associated with the binding of the reductase TMX1 to SERCA as previously published (*19*).

Although calnexin knockout MEFs showed higher levels of the SERCA inhibitor TMX1 (Fig. 5A), this was not the case with HeLa cells transfected with calnexin RNAi (fig. S3A), despite a similar $Ca^{2+}$ phenotype, thus ruling out the idea that the effects were due to altered TMX1 levels.

Overall, therefore, although TMX1 inactivates SERCA and promotes OXPHOS (*19*), in the case of calnexin, SERCA activation is functionally linked to mitochondrial OXPHOS. In contrast, uncoupling protein 3 inhibits both SERCA and OXPHOS (*53*). These discrepant findings suggest that mere control of ER $Ca^{2+}$ handling is not sufficient to assign the role that a MAM protein could play in mitochondria metabolism. For calnexin, the phenotype we observed was a combination of overall reduced OXPHOS and an increase in Krebs cycle activity, the latter potentially an adaptation (see also below). A reason for the complexity of the phenotype in calnexin knockout MEFs could be that the amounts of $Ca^{2+}$ available within mitochondria depend on at least three factors: ER $Ca^{2+}$ content, the distance and tethering between the ER and mitochondria, and the $Ca^{2+}$ uptake and release capabilities of the ER and mitochondria. Cross-talk between these factors could complicate the metabolic readout and compensatory mechanisms may nullify effects. For instance, SOCE could interfere with ER-mitochondria $Ca^{2+}$ cross-talk. Another possibility is a functional overlap between $Ca^{2+}$ handling and ER-mitochondria tethering. These two mechanisms can enter a positive feedback loop, because, on the one hand, $IP_3Rs$ not only release ER $Ca^{2+}$ but also are part of a tethering complex (*9*) and, on the other hand, increased release of ER $Ca^{2+}$ into the cytoplasm inhibits mitochondria movement (*37*, *38*). It appears that the main role of calnexin is to maintain ER $Ca^{2+}$ content, enabling the ER to maintain $IP_3R$-mediated $Ca^{2+}$ cross-talk that is critical for OXPHOS (*50*). At the same time, its activity to promote cytoplasmic $Ca^{2+}$ clearance reduces ER-mitochondria apposition. This role could also underlie the increased $\Delta\Psi$ responsiveness to $Ca^{2+}$ in calnexin knockout MEFs. Moreover, we observed increased $Ca^{2+}$ leak in the presence of calnexin. This could further alter $Ca^{2+}$ cross-talk and could also mitigate the effects we describe in our in silico model of ER-mitochondria apposition. The observed differences in ER-mitochondria apposition were substantive between calnexin wild-type and knockout MEFs.

In addition to $Ca^{2+}$ availability from the ER side of the MAM, mitochondrial $Ca^{2+}$ uptake and release can also determine the extent of mitochondrial ATP production through interference with $Ca^{2+}$ handling at the mitochondrial membranes. For instance, cells lacking the mitochondrial $Ca^{2+}$ uniporter (MCU) cannot ramp up energy production during stress (*54*). In contrast, a deletion of the

mitochondrial $Na^+/Ca^{2+}$ exchanger results in increased production of superoxide and ultimately apoptosis (*55*).

Based on our findings, the manipulation of $Ca^{2+}$ handling at the level of the ER is an important avenue to control the balance between OXPHOS and glycolysis. Calnexin executes such a function primarily through control of SERCA redox but might also control SERCA amounts through a chaperoning function. The relative importance and potential connection of these two functions could depend on the cell system or baseline redox conditions used, which could explain earlier findings (*26*). Moreover, the calnexin-mediated control of Nox4 and Ero1α/β activities could be especially critical in migrating endothelial cells, where Nox4 is upstream of SERCA oxidation upon incubation with vascular endothelial growth factor (*56*). Consistent with both findings, the antioxidant NAC fully reduced SERCA and eliminated redox control of OXPHOS in a calnexin-dependent manner (Fig. 6E). Other SERCA redox regulatory proteins exist, such as p53, which interacts with SERCA on ER-mitochondria contact sites and activates it by controlling its oxidation. In contrast to the oxidation-preserving role of calnexin, p53 prevents hyperoxidation of SERCA. Nevertheless, the consequences of this redox function are similar, because p53 thus also acts to preserve ER-mitochondria $Ca^{2+}$ flux and, as a consequence, mitochondrial apoptosis induction (*23*) and OXPHOS (*57*).

Thus, our results presented in this study suggest that calnexin could play a role for tumor cell metabolism, as suggested by our experiments in HeLa cells. Because high amounts of calnexin have been found in lung cancer and have been implicated as a poor prognostic marker in colorectal cancer (*58*, *59*), we propose that calnexin would increase cancer cell viability by maintaining OXPHOS in these scenarios, as has been shown for $IP_3Rs$ (*60*), a possibility that warrants future research. Calnexin has also been implicated in neurodegeneration, where its deficiency leads to neuronal dysmyelination but blocks neuroinflammation (*61*). Because inflammation could depend on the formation of functional MAMs (*62*), the described imbalance of this structure and the absence of mitochondrial ROS in calnexin knockout cells could provide an explanation.

## MATERIALS AND METHODS

### Antibodies and reagents

Basic chemicals were from Sigma-Aldrich (Oakville, ON). The following chemicals were purchased as indicated: reduced form of nicotinamide adenine dinucleotide (NADH), ATP, tert-BuBHQ, thapsigargin, Fura-2, Fluo-8, FCCP, tetramethylrhodamine methyl ester (TMRM), 2,7-dichlorofluorescein diacetate (DCF), BAPTA-AM, MitoSOX, CellROX, Oligofectamine, MitoTracker Green and Red (Thermo Fisher Scientific, Waltham, MA), oligomycin (Sigma-Aldrich, Oakville, ON), EN460 (Sigma-Aldrich, Oakville, ON), GKT137648 (Cayman, Ann Arbor, MI), and Percoll (GE Healthcare, Piscataway, NJ). Antibodies were purchased as indicated: against hexokinase 1 (Cell Signaling, Danvers, MA), hexokinase 2 (Cell Signaling, Danvers, MA), glyceraldehyde-3-phosphate dehydrogenase (GAPDH) (Cell Signaling, Danvers, MA), protein disulfide isomerase (PDI) (Pierce/Fisher, Rockford, IL), pyruvate dehydrogenase (PDH) (Cell Signaling, Danvers, MA), pyruvate kinase isozyme M2 (PKM2) (Cell Signaling, Danvers, MA), glucose transporter 1 (GLUT1) (GeneTex, Irvine, CA), GLUT4 (Abcam, Cambridge, MA), mitochondrial complex 2 (Cell Signaling, Danvers, MA), MCU (Sigma-Aldrich, Oakville, ON), mitofusin-2 (Sigma-Aldrich, Oakville, ON), VDAC1 (Abcam, Cambridge, MA), $IP_3R1$ (Thermo Fisher Scientific, Waltham, MA), PERK (Cell Signaling, Danvers, MA), p-PERK (Cell Signaling, Danvers, MA), ERp57 (StressMarq, Victoria, BC, Canada), NOX4 (Abcam, Cambridge, MA), AMPK (EMD Millipore, Billerica, MA), p-AMPK (EMD Millipore, Billerica, MA), SERCA2b (EMD Millipore, Billerica, MA), p62 (BD Biosciences, Franklin Lakes, NJ), actin (Thermo Fisher Scientific, Waltham, MA), tubulin (Sigma-Aldrich, Oakville, ON), IP3R2 (Alomone, Jerusalem, Israel), IP3R3 (BD Biosciences, Franklin Lakes, NJ), and FACL4 (Abcam, Cambridge, MA). The affinity-purified rabbit TMX1 antiserum was generated by 21st Century Biochemicals (Marlborough, MA) using a peptide corresponding to amino acids 251 to 271 (AES KEGTNKDFPQNAIRQRSL). The rabbit calnexin antibody has been previously described (*63*). HeLa cells were from ECACC (Porton Down, UK).

### Mathematical modeling

A mathematical model that considers the $Ca^{2+}$ cross-talk within the ER-mitochondria microdomain was used to develop a modified model to account for the effect of calnexin on cytosolic $Ca^{2+}$ oscillations and ER-mitochondria distance (*33*). First, the positive regulatory role of calnexin on the SERCA pump activity was described by an activating Hill function

$$V_{SERCA} = V_{SERCA0}\left(1 + \frac{[CNX]^4}{K_{COS}{}^4 + [CNX]^4}\right)$$

where $V_{SERCA}$ and $V_{SERCA0}$ are the actual activity and basic activity of SERCA pump, respectively. $V_{SERCA}$ was called the maximum SERCA activity in the original model (*33*). [CNX] is the concentration of calnexin, and $K_{COS}$ is the half-saturation constant with $K_{COS}$ = 0.03 μM. Second, considering that the maximal movement of mitochondria appears at resting $[Ca^{2+}]_{Cyt}$ with diminished motility during $[Ca^{2+}]_{Cyt}$ oscillations (*38*), we incorporated the dependence of ER-mitochondria distance on $[Ca^{2+}]_{Cyt}$ by a repressive Hill function

$$r = r_0 + r_c\left(\frac{K_{DOC}{}^4}{K_{DOC}{}^4 + [Ca^{2+}]_{Cyt}{}^4}\right)$$

Here, $r$ is the actual distance between ER and IMM, $r_0$ is the minimal ER-IMM distance, and $r_c$ is the maximal modulatory distance (set at 35 nm), which we multiply with a factor that accounts for changes of $[Ca^{2+}]_{Cyt}$ during waves on the ER-IMM distance. $K_{DOC}$ is the half-saturation constant with $K_{DOC}$ = 0.35 μM (*36*).

### Light membrane fractionation

Light membranes were separated as described previously (*63*). MEF cells were grown to 80% confluency on 10-cm dishes and treated as described in each experiment. Then, cells were washed twice with phosphate-buffered saline (PBS), harvested in 600 μl of cold homogenization buffer [250 mM sucrose, 10 mM Hepes-OH (pH 7.4), 1 mM EDTA, and 1 mM EGTA] + protease inhibitors (cOmplete, Roche), and homogenized by passing them seven times through a 26½ G needle. The resulting cell lysates were centrifuged at 800*g* for 10 min to remove nuclei and unbroken cells. The heavy membrane fraction was separated by centrifuging the postnuclear lysates at 10,000*g* for 10 min. The light membrane fraction was obtained by centrifuging the remaining supernatant at 60,000*g* for 1 hour and resuspending the pellet in 300 μl of 50 mM Hepes (pH 7.4), 125 mM NaCl, and 1 mM $MgCl_2$.

### MAM fractionation

MEFs were grown in fifteen 20-cm dishes, scraped with 5 ml of homogenization buffer [0.25 M sucrose, 10 mM Hepes-NaOH (pH 7.4), 1 mM EDTA, and 1 mM EGTA, containing cOmplete protease inhibitor; Roche, Mississauga, ON], centrifuged at 300*g* for 5 min, and resuspended in 5 ml of homogenization buffer. Then, cells were homogenized with seven passages through a ball-bearing homogenizer (Isobiotec, Heidelberg, Germany, ball clearance 18 μM). The resulting homogenate was centrifuged for 10 min at 600*g* to remove unbroken cells and nuclei. Postnuclear supernatant was centrifuged for 10 min at 8500*g* to yield the crude mitochondria fraction. The supernatant was then centrifuged for 60 min at 60,000*g* to separate the cytosolic fraction and microsome fraction. The previously isolated crude mitochondria fraction was resuspended in 1 ml of homogenization buffer and layered on top of 7.9 ml of 18% v/v Percoll in homogenization buffer and centrifuged for 30 min at 30,000*g*. Purified MAM and pure mitochondria fraction bands were extracted from the gradient using a syringe. The band containing the MAM fraction was centrifuged for 1 hour at 95,000*g* to yield the MAM fraction. The band containing the pure mitochondria fraction was centrifuged for 10 min at 10,000*g* to yield the pure mitochondria fraction. The cytosolic fraction was precipitated overnight with acetone and centrifuged for 20 min at 16,000*g*. All fractions were resuspended in loading buffer [60 mM tris-HCl (pH 6.8), 2% SDS, 10% glycerol, 10% β-mercaptoethanol, and 0.004% bromophenol blue] and equal proportional amounts were analyzed by Western blotting.

### ATPase assay

The ATPase assay was carried out using an enzyme coupled reaction in which the regeneration of ATP is coupled to the oxidation of NADH, as previously described (*64*). Activity was detected as a decrease in NADH absorbance at 340 nm, which was measured every 1 min for 120 min using a microplate reader (Synergy, BioTek) and the path-length correction function. All reactions were carried out in triplicate in a final volume of 100 μl using a 96-well plate. The decrease in NADH absorbance at 340 nm was converted to micromoles of ATP using Beer's law and then expressed as a function of time. The final conditions for all the reactions were 25 mM Hepes (pH 7.2), 125 mM NaCl, 5 mM $MgCl_2$, 0.1 mM $CaCl_2$, 1 mM DTT, 0.6 mM NADH, 2 mM ATP, 1 mM phosphoenol pyruvate, 2.5 μl of pyruvate kinase/lactate dehydrogenase (Sigma-Aldrich), and 0.02% dimethyl sulfoxide. Identical reactions were treated with 10 μM thapsigargin and subtracted from untreated reactions to identify specific SERCA activity. Protein concentration of light membrane samples was quantified using the Pierce BCA Protein Assay Kit and 1 μg of protein was added to each well. Reactions were started by adding the regenerating system consisting of DTT, NADH, ATP, phosphoenol pyruvate, and pyruvate kinase/lactate dehydrogenase to the resuspended light membranes. Fit lines were calculated with the following equation: $Y = ((B_{max} * X)/(K_{app} + X)) + X_0$. SERCA ATPase activity is shown as the percentage of the ATPase activity inhibited by thapsigargin in the light membranes and as ATPase activity per microgram of protein in the light membranes.

### Cell lysates and Western blotting

MEFs were grown to 80% confluency on 60-mm dishes, washed twice with PBS, and harvested in 300 μl of cold CHAPS buffer [10 mM tris (pH 7.4), NaCl 150 mM, 1 mM EDTA, and 1% CHAPS] + protease inhibitors (cOmplete, Roche) + phosphatase inhibitors (PhosSTOP, Roche). After centrifuging at 800*g* for 10 min to remove nuclei and unbroken cells, the lysate was mixed with loading buffer [60 mM tris-HCl (pH 6.8), 2% SDS, 10% glycerol, 10% β-mercaptoethanol, and 0.004% bromophenol blue]. Equal amounts of protein per sample were loaded and separated by SDS–polyacrylamide gel electrophoresis (SDS-PAGE) (10% acrylamide gels) and transferred to nitrocellulose membranes. Membranes were blocked with blocking buffer [10 mM tris (pH 8), 150 mM NaCl, 0.05% Triton X-100, and 2% bovine serum albumin (BSA)] and incubated with primary antibodies overnight. The next day, membranes were incubated with secondary antibodies and proteins were detected using a LI-COR imaging system (Biosciences). Band intensity was quantified using the Fiji (*65*) distribution of ImageJ 1.52b (*66*).

### Microscopy and image acquisition

Microscopy experiments were performed on an FV1000 laser-scanning confocal microscope (Olympus) using a 60× objective [XLUMPLANFL, numerical aperture (NA) 1.0; Olympus] or a 20× objective (XLUMPLANFL, NA 1.0; Olympus), equipped with a perfusion system consisting of a peristaltic pump (for the FV1000 system, Watson-Marlow Alitea-AB; Sin-Can). Live-cell images were taken with a 559-nm laser excitation with a 575- to 675-nm bandpass emission filter for MitoTracker Red, ER R-GECO (LAR-ER-GECO), mitochondrial R-GECO, and TMRM fluorescent probes, and a 473-nm laser excitation with a 490- to 540-nm bandpass emission filter for SPLICS-short, SPLICS-long, FLUO8, and MitoTracker Green using a PL-A686 6.6 megapixel camera (Capture SE software, Pixelink). The temperature in the recording chamber was kept at 25° to 27°C (TC-324B, Harvard Apparatus). Cells were incubated in tissue culture medium supplemented with drugs as indicated. Fluorochromes were used as indicated. Images were acquired with Olympus FluoView software. Image analysis and mitochondrial particle quantification were done with the Fiji (*65*) distribution of ImageJ 1.52b (*66*) using the Time Series Analyzer v3.0 plugin for measurements over time.

### ER and mitochondrial $Ca^{2+}$ measurements

To measure ER and mitochondrial $Ca^{2+}$, we used the low-affinity ER R-GECO (LAR-ER-GECO) and the mitochondrial R-GECO fluorescent $Ca^{2+}$ indicators (*40*). To express these $Ca^{2+}$ indicators, MEFs were transfected with plasmids containing the corresponding fluorescent probe using Nucleofector 2b Device (Lonza, AAB-1001) and the MEF 1 Nucleofector Kit (Amaxa, catalog number VPD-1004). Following the manufacturer's instructions, $2 \times 10^6$ MEFs were transfected with 5 μg of plasmid containing the corresponding probe using the A-023 program. Transfected cells were seeded in poly-L-lysine–coated coverslips (12 mm) in 24-well plates (300,000 cells per well). The next day, coverslips were transferred to the microscope and perfused with Hanks' balanced salt solution (HBSS) with $Ca^{2+}$ and $Mg^{2+}$ (HBSS/Ca/Mg) at 5 ml/min. Live-cell images were taken every 3 s with a 559-nm laser excitation and a 575- to 675-nm bandpass emission filter. After establishment of a 30-s baseline, the perfusion medium was changed to HBSS/Ca/Mg + ATP 100 μM for 5 min or HBSS without $Ca^{2+}$ + TBHQ 60 μM for 10 min, and the experiment was continued for 5 to 10 min using HBSS/Ca/Mg or HBSS without $Ca^{2+}$, respectively. Independent experiments consisted of 10 to 20 cells.

### SOCE measurements

Cells were seeded in poly-L-lysine–coated coverslips (12 mm) in 24-well plates (50,000 cells per well). Then, the next day, cells were incubated with FLUO8 1 μM for 30 min. The coverslips were transferred to the microscope and perfused with HBSS with $Ca^{2+}$ and $Mg^{2+}$ (Thermo Fisher Scientific, catalog number 14025) (HBSS/Ca/Mg) at 5 ml/min. Live-cell images were taken every 5 s with a 473-nm laser excitation with a 490- to 540-nm bandpass emission filter. After establishment of a 30-s baseline, the perfusion medium was changed to HBSS without $Ca^{2+}$ but containing 10 μM thapsigargin. After 10 min, the perfusion medium was changed to HBSS/Ca/Mg for 10 min. Independent experiments consisted of 20 to 30 cells.

### Mitochondrial membrane potential

Cells were seeded in poly-L-lysine–coated coverslips (12 mm) in 24-well plates (50,000 cells per well). The next day, cells were incubated with 40 nM TMRM for 30 min. Then, coverslips were transferred to the microscope and perfused with HBSS with $Ca^{2+}$ and $Mg^{2+}$ (Thermo Fisher Scientific, catalog number 14025) (HBSS/Ca/Mg) at 5 ml/min. Live-cell images were taken every 5 s with a 559-nm laser excitation and a 575- to 675-nm bandpass emission filter. After establishment of a 30-s baseline, the perfusion medium was changed to HBSS/Ca/Mg + 10 μM FCCP for 10 min. Independent experiments consisted of 20 to 30 cells.

### Cytoplasmic measurements of $Ca^{2+}$ release

To measure ER $Ca^{2+}$ release into the cytosol, we used the fluorescent $Ca^{2+}$ probe Fura-2. MEFs were seeded in 60-mm dishes at a concentration of $2 \times 10^6$ cells per dish. The next day, cells were washed with HBSS buffer with $Ca^{2+}$ and $Mg^{2+}$ (Thermo Fisher Scientific, catalog number 14025) and 0.1% BSA (HBSS/Ca/Mg/BSA) and then incubated with 1.5 ml of 1 μM Fura-2 in HBSS/Ca/Mg/BSA for 30 min at room temperature in the dark. Next, we replaced the loading medium with HBSS/Ca/Mg/BSA and incubated it for a further 15 min in the dark. After trypsinization and quenching with 1 ml of Dulbecco's modified Eagle's medium (DMEM)/10% fetal bovine serum (FBS), cells were washed twice with 1 ml of HBSS/Ca/Mg/BSA. Cells were then resuspended in HBSS/Ca/Mg/BSA and transferred into a cuvette containing a stirring bar, and 505-nm emissions were measured with 340/380 nm excitation on an 814 photomultiplier detection system (PTI), upon establishment of a 200-s baseline. Drugs (50 μM histamine or 10 μM thapsigargin) were added as 100 μl of a 200× stock solution prepared in HBSS/Ca/Mg/BSA. The $Ca^{2+}$ response was determined as the relative ratiometric signal obtained from the baseline and after adding drugs. For the decay calculation, we fit a line into the data derived from the peak until 30 s later.

### Electron microscopy

Cell monolayers were fixed for 20 min using 2% paraformaldehyde and 2% glutaraldehyde in 100 mM sodium cacodylate buffer at pH 7.4. Cells were scraped from the plates and pelleted. Secondary fixation was in osmium tetroxide 1% followed by quick rinses in water and staining in 1% aqueous solution of uranyl acetate. Dehydration was in increasing concentrations of ethanol and was followed by incubation in propylene oxide at room temperature. Pellets were infused with Embed 812 and blocks were hardened at 60°C for a minimum of 48 hours. We used an Ultracut E, Reichert-Jung for sectioning and imaged the samples using a charge-coupled device (CCD) camera (iTEM, Olympus Soft Imaging Solutions) mounted on a Philips 410 TEM. On the images, we identified ER tubules in close proximity to mitochondria and determined their distance in nanometers. We recorded apposed ER tubules per mitochondrion (distance <50 nm) and quantified their distance and length.

### SPLICS

MEF cells were transfected with plasmids containing the SPLICS-long or SPLICS-short probes using Nucleofector 2b Device (Lonza, AAB-1001) and the MEF 1 Nucleofector Kit (Amaxa, catalog number VPD-1004). Following the manufacturer's instructions, $2 \times 10^6$ MEFs were transfected with 5 μg of plasmid containing the corresponding probe using the A-023 program. Transfected cells were seeded in poly-L-lysine–coated coverslips (12 mm) in 24-well plates (300,000 cells per well). Forty-eight hours later, cells were treated with NAC 5 mM for 4 hours, stained with MitoTracker Red 1 μM for 30 min at 37°C, and fixed with 4% paraformaldehyde for 20 min at room temperature. Cells were imaged using a laser scanning confocal microscope with a 60× objective (XLUMPLANFL, NA 1.0; Olympus). Images were convolved, filtered using a Gaussian Blur filter, and thresholded (*39*). SPLICS particles were quantified using ImageJ.

### Total ATP determination

Cellular ATP content was determined using the ATP Determination kit (Molecular Probes, A22066) based on a luciferase enzymatic reaction. MEFs were seeded in six-well plates at a concentration of 500,000 cells per well. The next day, cells were treated as described in each experiment. Then, cells were trypsinized and 600,000 viable cells were centrifuged and resuspended in CHAPS buffer [10 mM tris (pH 7.4), NaCl 150 mM, 1 mM EDTA, and 1% CHAPS] + protease inhibitors (cOmplete, Roche). Luminescence was measured using Lumat LB 9507 (Berthold Technologies) at 560 nm.

### Oxygen consumption rates

The respiratory capacity of the mitochondrial electron transport chain was measured in intact cells using high-resolution respirometry (Oxygraph-2K; Oroboros), as previously described (*67*). MEFs were seeded in 60-mm dishes at a concentration of $2 \times 10^6$ cells per dish. The next day, cells were trypsinized, centrifuged at 100*g* for 5 min, and resuspended in culture media at a cell density of $10^6$ cells/ml. Basic parameters of mitochondrial function were assessed at 37°C and expressed as pmol $O_2$/s/citrate synthase activity in a single protocol designed to assess basal respiration, ATP turnover respiration (after addition of the ATP synthase inhibitor oligomycin), and maximal respiration (or electron transfer system capacity, after addition of the protonophoric uncoupler carbonyl cyanide-4-[trifluoromethoxy] phenylhydrazone). All respiratory rates were corrected for non-mitochondrial respiration (2.5 μM antimycin-inhibited rate) (*68*).

### Citrate synthase activity

The activity of the mitochondrial enzyme citrate synthase was quantified by measuring the formation of thionitrobenzoate from 5,5-dithiobis-2-nitrobenzoate after the addition of 0.3 mM acetyl-coenzyme A and 0.5 mM oxaloacetate. The production on thionitrobenzoate was measured spectrophotometrically at 412 nm for 2 min.

### Mitochondrial area

Cells were seeded in poly-L-lysine–coated coverslips (12 mm) in 24-well plates (50,000 cells per well). The next day, cells were incubated with 1 μM MitoTracker Green for 30 min at 37°C. Coverslips were

perfused with HBSS with $Ca^{2+}$ and $Mg^{2+}$ (HBSS/Ca/Mg). Live cells were imaged using a laser scanning confocal microscope with a 60× objective (XLUMPLANFL, NA 1.0; Olympus). A background threshold was subtracted from images, and mitochondrial particles were quantified using ImageJ.

### Metabolomics

Cells were seeded in 10-cm dishes ($2 \times 10^6$ cells per dish). The next day, culture medium was replaced with 7 ml of fresh culture medium with the indicated inhibitors. After 24 hours, culture medium was filtered with 0.2-μm filters and mixed with the dextran sulfate sodium (DSS) reference solution. Nuclear magnetic resonance (NMR) spectroscopy was performed at the NANUC National High Field NMR Facility using a 2.2-K pumped 800-MHz Oxford magnet updated to a Bruker Neo-Advance IV console equipped with a 5-mm cryoprobe. One-dimensional NMR spectra were collected at 25°C using the standard noesypr1d pulse sequence with a transmitter presaturation delay of 990 ms for water suppression, a 100-ms mixing time, 8 steady-state scans, and a spectral width of 12 ppm. The total acquisition time was 4 s per transient, with 128 transients acquired per sample. The raw data were processed using the Chenomx Processor module from the Chenomx NMR suite. The free induction decays were apodized with an exponential window function corresponding to a line broadening of 0.1 Hz, zero-filled to 128K complex points, Fourier-transformed, phased, and baseline-corrected for further analysis. Reference deconvolution using the methyl peak of DSS as the reference peak was used to correct for line shapes. Metabolites were quantified using the Chenomx NMR Suite software (version 8.4) application developed by Chenomx Inc. (Edmonton, AB, Canada).

### Mitochondrial ATP measurements

Before fluorescence microscopic experiments, cells were equilibrated for at least 30 min in a buffer composed of 2 mM $CaCl_2$, 135 mM NaCl, 1 mM $MgCl_2$, 5 mM KCl, 10 mM Hepes, 2.6 mM $NaHCO_3$, 0.44 mM $KH_2PO_4$, 0.34 mM $Na_2HPO_4$, 1× amino acids, 1× vitamins, 10 mM glucose, and 2 mM L-glutamine with a pH of 7.45. During microscopic experiments, cells were perfused using buffers composed of 2 mM $CaCl_2$, 138 mM NaCl, 1 mM MgCl, 5 mM KCl, and 10 mM Hepes with or without 10 mM glucose, with or without 3 μM Oligomycin-A. Buffers were exchanged using a gravity-based perfusion system (NGFI GmbH, Graz, Austria).

Mitochondrial ATP dynamics of MEFs were assessed using mtAT1.03. MEFs were analyzed at an OLYMPUS IX73 inverted microscope (OLYMPUS, Vienna, Austria) using a 40× objective (UApo N 340, 40×/1.35 Oil, ∞/0.17/FN22, OLYMPUS). Illumination was performed using an OMICRON LedHUB High-Power light-emitting diode (LED) light engine, equipped with a 455-nm LED light source (OMICRON electronics, Vienna, Austria), and a 430-nm excitation filter (AHF Analysentechnik, Tübingen, Germany). Images were captured at a binning of 4 using a Retiga R1 CCD camera (Teledyne QImaging, Surrey, Canada), and emissions were separated using an optical beam splitter (DV2, Photometrics, Arizona, USA). Device control and image acquisition was performed using VisiView image acquisition and control software (Visitron Systems, Puchheim, Germany).

### ROS measurements

Mitochondrial ROS levels were measured using MitoSOX (Molecular Probes, M36008), and cellular ROS levels were measured using CellROX (Molecular Probes, C10443). MEFs were seeded in six-well plates at a concentration of 500,000 cells per well. The next day, MEFs were treated with 5 μM MitoSOX for 10 min at 37°C or 5 μM CellROX for 30 min. After trypsinization and quenching with 1 ml of DMEM/10% FBS, cells were centrifuged at 100*g* for 5 min and resuspended in HBSS buffer with $Ca^{2+}$ and $Mg^{2+}$ (Thermo Fisher Scientific, catalog number 14025) and 0.1% BSA (HBSS/Ca/Mg/BSA). MitoSOX fluorescence signal (excitation 510/emission 580 nm) and CellROX (excitation 545/emission 565 nm) were measured using flow cytometry (LSRFortessa, BD).

### SERCA redox state

Cells were transfected with Myc-SERCA for 24 hours before incubation with 10 mM DTT for 10 min, 5 mM diamide for 5 min, or no treatment, respectively, at 37°C. Cells were rinsed with warm PBS twice, lysed with BIAM (Thermo Fisher Scientific, 21334) reaction buffer [50 mM tris-HCl (pH 8), 50 mM NaCl, 5 mM EDTA, 1% Triton X-100, 0.1% IGEPAL CA-630, 200 μM BIAM, and Roche EDTA-free protease inhibitors], and centrifuged at 10,000*g* for 5 min. Samples were incubated at 25°C for 90 min in the dark to allow biotinylation of reduced proteins. Unreacted BIAM was removed by Bio-Spin P-6 columns (Bio-Rad, 732-6221) with buffer exchanged to CHAPS buffer [1% CHAPS, 10 mM tris-HCl (pH 7.4), 150 mM NaCl, 1 mM EDTA, and Roche EDTA-free protease inhibitors]. Immunoprecipitation of Myc-SERCA was performed by rocking the samples with mouse c-Myc antibody (Thermo Scientific, 13-2500) at 4°C overnight, followed by 1 hour of rocking with Protein G Sepharose beads (GE Healthcare, 17-0618-01). Beads were washed four times with CHAPS buffer before boiling with 2× sample loading buffer containing 50 mM DTT. Samples were subjected to SDS-PAGE. Biotinylated SERCA and Myc-SERCA were visualized by immunoblotting using goat biotin antibody (Sigma-Aldrich B3640) and rabbit Myc antibody (Millipore 06-549), respectively.

### CNX knockdown

HeLa cells were transfected with siCtrl or siCNX (Stealth Select RNAi, CANX HSS188690, control Stealth siRNA, Thermo Fisher Scientific) using Oligofectamine (Thermo Fisher Scientific). Cells were seeded in six-well plates ($1 \times 10^6$ cells per well). The next day, cells were transfected following the manufacturer's instructions. Experiments were performed 48 hours after transfection.

### Data analysis

Data were analyzed using LibreOffice Calc 6.0 and R 3.5 (with RStudio 1.1). Data normality was determined with Shapiro-Wilk test and visual examination of QQ plots. Equality of variances between samples was determined with Levene's test. Normally distributed data were analyzed with *t* test, and data with non-normal distribution were analyzed with Wilcoxon test. One-sample *t* test and one-sample Wilcoxon test were used to compare the differences between one sample and a normalized control (for example, to 100%). Two-sample *t* test and two-sample Wilcoxon test were used to compare two samples, with the corresponding adjustment depending on the equality of variances. The Holm adjustment method was used to compare the differences between more than two samples.

## SUPPLEMENTARY MATERIALS

stke.sciencemag.org/cgi/content/full/13/638/eaax6660/DC1

Fig. S1. Additional controls and $Ca^{2+}$ modeling.

Fig. S2. Additional ER and mitochondria $Ca^{2+}$ and metabolic measurements.

Fig. S3. Additional biochemical analyses.
Fig. S4. NAC modulation of metabolic characteristics in HeLa cells.
Fig. S5. Analysis of ROS sources.

View/request a protocol for this paper from *Bio-protocol*.

## REFERENCES AND NOTES


1. W. Bernhard, F. Haguenau, A. Gautier, C. Oberling, La structure submicroscopique des elements basophiles cytoplasmiques dans le foie, le pancreas et les glandes salivaires. *Z. Zellforsch. Mikrosk. Anat.* **37**, 281–300 (1952).
2. W. Bernhard, C. Rouiller, Close topographical relationship between mitochondria and ergastoplasm of liver cells in a definite phase of cellular activity. *J. Biophys. Biochem. Cytol.* **2**, 73–78 (1956).
3. D. W. Fawcett, Observations on the cytology and electron microscopy of hepatic cells. *J. Natl. Cancer Inst.* **15**, 1475–1503 (1955).
4. A. Sood, D. V. Jeyaraju, J. Prudent, A. Caron, P. Lemieux, H. M. McBride, M. Laplante, K. Tóth, L. Pellegrini, A Mitofusin-2-dependent inactivating cleavage of Opa1 links changes in mitochondria cristae and ER contacts in the postprandial liver. *Proc. Natl. Acad. Sci. U.S.A.* **111**, 16017–16022 (2014).
5. P. Theurey, E. Tubbs, G. Vial, J. Jacquemetton, N. Bendridi, M. A. Chauvin, M. R. Alam, M. le Romancer, H. Vidal, J. Rieusset, Mitochondria-associated endoplasmic reticulum membranes allow adaptation of mitochondrial metabolism to glucose availability in the liver. *J. Mol. Cell Biol.* **8**, 129–143 (2016).
6. J. Rieusset, The role of endoplasmic reticulum-mitochondria contact sites in the control of glucose homeostasis: An update. *Cell Death Dis.* **9**, 388 (2018).
7. R. J. Kaufman, J. D. Malhotra, Calcium trafficking integrates endoplasmic reticulum function with mitochondrial bioenergetics. *Biochim. Biophys. Acta* **1843**, 2233–2239 (2014).
8. B. Kornmann, E. Currie, S. R. Collins, M. Schuldiner, J. Nunnari, J. S. Weissman, P. Walter, An ER-mitochondria tethering complex revealed by a synthetic biology screen. *Science* **325**, 477–481 (2009).
9. G. Szabadkai, K. Bianchi, P. Várnai, D. De Stefani, M. R. Wieckowski, D. Cavagna, A. I. Nagy, T. Balla, R. Rizzuto, Chaperone-mediated coupling of endoplasmic reticulum and mitochondrial $Ca^{2+}$ channels. *J. Cell Biol.* **175**, 901–911 (2006).
10. J. G. Wideman, D. L. Balacco, T. Fieblinger, T. A. Richards, PDZD8 is not the 'functional ortholog' of Mmm1, it is a paralog. *F1000Res* **7**, 1088 (2018).
11. Y. Hirabayashi, S. K. Kwon, H. Paek, W. M. Pernice, M. A. Paul, J. Lee, P. Erfani, A. Raczkowski, D. S. Petrey, L. A. Pon, F. Polleux, ER-mitochondria tethering by PDZD8 regulates $Ca^{2+}$ dynamics in mammalian neurons. *Science* **358**, 623–630 (2017).
12. T. Simmen, E. M. Lynes, K. Gesson, G. Thomas, Oxidative protein folding in the endoplasmic reticulum: Tight links to the mitochondria-associated membrane (MAM). *Biochim. Biophys. Acta* **1798**, 1465–1473 (2010).
13. T. Gutiérrez, T. Simmen, Endoplasmic reticulum chaperones tweak the mitochondrial calcium rheostat to control metabolism and cell death. *Cell Calcium* **70**, 64–75 (2018).
14. S. Y. Gilady, M. Bui, E. M. Lynes, M. D. Benson, R. Watts, J. E. Vance, T. Simmen, Ero1alpha requires oxidizing and normoxic conditions to localize to the mitochondria-associated membrane (MAM). *Cell Stress Chaperones* **15**, 619–629 (2010).
15. T. Higo, M. Hattori, T. Nakamura, T. Natsume, T. Michikawa, K. Mikoshiba, Subtype-specific and ER lumenal environment-dependent regulation of inositol 1,4,5-trisphosphate receptor type 1 by ERp44. *Cell* **120**, 85–98 (2005).
16. I. T. Cho, G. Adelmant, Y. Lim, J. A. Marto, G. Cho, J. A. Golden, Ascorbate peroxidase proximity labeling coupled with biochemical fractionation identifies promoters of endoplasmic reticulum-mitochondrial contacts. *J. Biol. Chem.* **292**, 16382–16392 (2017).
17. V. Hung, S. S. Lam, N. D. Udeshi, T. Svinkina, G. Guzman, V. K. Mootha, S. A. Carr, A. Y. Ting, Proteomic mapping of cytosol-facing outer mitochondrial and ER membranes in living human cells by proximity biotinylation. *eLife* **6**, e24463 (2017).
18. E. M. Lynes, A. Raturi, M. Shenkman, C. O. Sandoval, M. C. Yap, J. Wu, A. Janowicz, N. Myhill, M. D. Benson, R. E. Campbell, L. G. Berthiaume, G. Z. Lederkremer, T. Simmen, Palmitoylation is the switch that assigns calnexin to quality control or ER $Ca^{2+}$ signaling. *J. Cell Sci.* **126**, 3893–3903 (2013).
19. A. Raturi, T. Gutiérrez, C. Ortiz-Sandoval, A. Ruangkittisakul, M. S. Herrera-Cruz, J. P. Rockley, K. Gesson, D. Ourdev, P. H. Lou, E. Lucchinetti, N. Tahbaz, M. Zaugg, S. Baksh, K. Ballanyi, T. Simmen, TMX1 determines cancer cell metabolism as a thiol-based modulator of ER-mitochondria $Ca^{2+}$ flux. *J. Cell Biol.* **214**, 433–444 (2016).
20. X. Zhang, C. S. Gibhardt, T. Will, H. Stanisz, C. Körbel, M. Mitkovski, I. Stejerean, S. Cappello, D. Pacheu-Grau, J. Dudek, N. Tahbaz, L. Mina, T. Simmen, M. W. Laschke, M. D. Menger, M. P. Schön, V. Helms, B. A. Niemeyer, P. Rehling, A. Vultur, I. Bogeski, Redox signals at the ER-mitochondria interface control melanoma progression. *EMBO J.* **38**, e100871 (2019).
21. E. D. Lagadinou, A. Sach, K. Callahan, R. M. Rossi, S. J. Neering, M. Minhajuddin, J. M. Ashton, S. Pei, V. Grose, K. M. O'Dwyer, J. L. Liesveld, P. S. Brookes, M. W. Becker, C. T. Jordan, BCL-2 inhibition targets oxidative phosphorylation and selectively eradicates quiescent human leukemia stem cells. *Cell Stem Cell* **12**, 329–341 (2013).
22. G. Manfredi, J. Q. Kwong, J. A. Oca-Cossio, M. Woischnik, C. D. Gajewski, K. Martushova, M. D'Aurelio, A. L. Friedlich, C. T. Moraes, BCL-2 improves oxidative phosphorylation and modulates adenine nucleotide translocation in mitochondria of cells harboring mutant mtDNA. *J. Biol. Chem.* **278**, 5639–5645 (2003).
23. C. Giorgi, M. Bonora, G. Sorrentino, S. Missiroli, F. Poletti, J. M. Suski, F. Galindo Ramirez, R. Rizzuto, F. di Virgilio, E. Zito, P. P. Pandolfi, M. R. Wieckowski, F. Mammano, G. del Sal, P. Pinton, p53 at the endoplasmic reticulum regulates apoptosis in a $Ca^{2+}$–dependent manner. *Proc. Natl. Acad. Sci. U.S.A.* **112**, 1779–1784 (2015).
24. S. Matoba, J. G. Kang, W. D. Patino, A. Wragg, M. Boehm, O. Gavrilova, P. J. Hurley, F. Bunz, P. M. Hwang, p53 regulates mitochondrial respiration. *Science* **312**, 1650–1653 (2006).
25. P. Stambolsky, L. Weisz, I. Shats, Y. Klein, N. Goldfinger, M. Oren, V. Rotter, Regulation of AIF expression by p53. *Cell Death Differ.* **13**, 2140–2149 (2006).
26. H. L. Roderick, J. D. Lechleiter, P. Camacho, Cytosolic phosphorylation of calnexin controls intracellular Ca(2+) oscillations via an interaction with SERCA2b. *J. Cell Biol.* **149**, 1235–1248 (2000).
27. P. Camacho, J. D. Lechleiter, Calreticulin inhibits repetitive intracellular $Ca^{2+}$ waves. *Cell* **82**, 765–771 (1995).
28. T. Adachi, R. M. Weisbrod, D. R. Pimentel, J. Ying, V. S. Sharov, C. Schöneich, R. A. Cohen, S-Glutathiolation by peroxynitrite activates SERCA during arterial relaxation by nitric oxide. *Nat. Med.* **10**, 1200–1207 (2004).
29. Y. Li, P. Camacho, $Ca^{2+}$–dependent redox modulation of SERCA 2b by ERp57. *J. Cell Biol.* **164**, 35–46 (2004).
30. A. Raturi, C. Ortiz-Sandoval, T. Simmen, Redox dependence of endoplasmic reticulum (ER) $Ca^{2+}$ signaling. *Histol. Histopathol.* **29**, 543–552 (2014).
31. J. T. Tuusa, T. T. Leskelä, U. E. Petäjä-Repo, Human delta opioid receptor biogenesis is regulated via interactions with SERCA2b and calnexin. *FEBS J.* **277**, 2815–2829 (2010).
32. S. R. Jaffrey, S. H. Snyder, The biotin switch method for the detection of S-nitrosylated proteins. *Sci. STKE* **2001**, pl1 (2001).
33. H. Qi, L. Li, J. Shuai, Optimal microdomain crosstalk between endoplasmic reticulum and mitochondria for $Ca^{2+}$ oscillations. *Sci. Rep.* **5**, 7984 (2015).
34. M. Giacomello, L. Pellegrini, The coming of age of the mitochondria-ER contact: A matter of thickness. *Cell Death Differ.* **23**, 1417–1427 (2016).
35. D. V. Jeyaraju, G. Cisbani, L. Pellegrini, Calcium regulation of mitochondria motility and morphology. *Biochim. Biophys. Acta* **1787**, 1363–1373 (2009).
36. M. Saotome, D. Safiulina, G. Szabadkai, S. Das, A. Fransson, P. Aspenstrom, R. Rizzuto, G. Hajnoczky, Bidirectional $Ca^{2+}$–dependent control of mitochondrial dynamics by the Miro GTPase. *Proc. Natl. Acad. Sci. U.S.A.* **105**, 20728–20733 (2008).
37. X. Wang, T. L. Schwarz, The mechanism of $Ca^{2+}$–dependent regulation of kinesin-mediated mitochondrial motility. *Cell* **136**, 163–174 (2009).
38. M. Yi, D. Weaver, G. Hajnoczky, Control of mitochondrial motility and distribution by the calcium signal: A homeostatic circuit. *J. Cell Biol.* **167**, 661–672 (2004).
39. D. Cieri, M. Vicario, M. Giacomello, F. Vallese, R. Filadi, T. Wagner, T. Pozzan, P. Pizzo, L. Scorrano, M. Brini, T. Calì, SPLICS: A split green fluorescent protein-based contact site sensor for narrow and wide heterotypic organelle juxtaposition. *Cell Death Differ.* **25**, 1131–1145 (2018).
40. J. Wu, D. L. Prole, Y. Shen, Z. Lin, A. Gnanasekaran, Y. Liu, L. Chen, H. Zhou, S. R. W. Chen, Y. M. Usachev, C. W. Taylor, R. E. Campbell, Red fluorescent genetically encoded $Ca^{2+}$ indicators for use in mitochondria and endoplasmic reticulum. *Biochem. J.* **464**, 13–22 (2014).
41. M. R. Depaoli, F. Karsten, C. T. Madreiter-Sokolowski, C. Klec, B. Gottschalk, H. Bischof, E. Eroglu, M. Waldeck-Weiermair, T. Simmen, W. F. Graier, R. Malli, Real-time imaging of mitochondrial ATP dynamics reveals the metabolic setting of single cells. *Cell Rep.* **25**, 501–512.e3 (2018).
42. K. K. Prior, I. Wittig, M. S. Leisegang, J. Groenendyk, N. Weissmann, M. Michalak, P. Jansen-Dürr, A. M. Shah, R. P. Brandes, The endoplasmic reticulum chaperone calnexin is a NADPH oxidase NOX4 interacting protein. *J. Biol. Chem.* **291**, 7045–7059 (2016).
43. H. G. Hansen, J. D. Schmidt, C. L. Søltoft, T. Ramming, H. M. Geertz-Hansen, B. Christensen, E. S. Sørensen, A. S. Juncker, C. Appenzeller-Herzog, L. Ellgaard, Hyperactivity of the Ero1α oxidase elicits endoplasmic reticulum stress but no broad antioxidant response. *J. Biol. Chem.* **287**, 39513–39523 (2012).
44. J. D. Malhotra, H. Miao, K. Zhang, A. Wolfson, S. Pennathur, S. W. Pipe, R. J. Kaufman, Antioxidants reduce endoplasmic reticulum stress and improve protein secretion. *Proc. Natl. Acad. Sci. U.S.A.* **105**, 18525–18530 (2008).
45. J. D. Blais, K. T. Chin, E. Zito, Y. Zhang, N. Heldman, H. P. Harding, D. Fass, C. Thorpe, D. Ron, A small molecule inhibitor of endoplasmic reticulum oxidation 1 (ERO1) with selectively reversible thiol reactivity. *J. Biol. Chem.* **285**, 20993–21003 (2010).
46. N. K. Somanna, A. J. Valente, M. Krenz, W. P. Fay, P. Delafontaine, B. Chandrasekar, The Nox1/4 dual inhibitor GKT137831 or Nox4 knockdown inhibits angiotensin-II-induced adult mouse cardiac fibroblast proliferation and migration. AT1 physically associates with Nox4. *J. Cell. Physiol.* **231**, 1130–1141 (2016).
47. R. Rizzuto, P. Pinton, W. Carrington, F. S. Fay, K. E. Fogarty, L. M. Lifshitz, R. A. Tuft, T. Pozzan, Close contacts with the endoplasmic reticulum as determinants of mitochondrial $Ca^{2+}$ responses. *Science* **280**, 1763–1766 (1998).

48. R. M. Denton, Regulation of mitochondrial dehydrogenases by calcium ions. *Biochim. Biophys. Acta* **1787**, 1309–1316 (2009).
49. G. Bustos, P. Cruz, A. Lovy, C. Cardenas, Endoplasmic reticulum-mitochondria calcium communication and the regulation of mitochondrial metabolism in cancer: A novel potential target. *Front. Oncol.* **7**, 199 (2017).
50. C. Cárdenas, R. A. Miller, I. Smith, T. Bui, J. Molgó, M. Müller, H. Vais, K.-H. Cheung, J. Yang, I. Parker, C. B. Thompson, M. J. Birnbaum, K. R. Hallows, J. K. Foskett, Essential regulation of cell bioenergetics by constitutive InsP3 receptor $Ca^{2+}$ transfer to mitochondria. *Cell* **142**, 270–283 (2010).
51. A. K. Lakkaraju, L. Abrami, T. Lemmin, S. Blaskovic, B. Kunz, A. Kihara, M. Dal Peraro, F. G. van der Goot, Palmitoylated calnexin is a key component of the ribosome-translocon complex. *EMBO J.* **31**, 1823–1835 (2012).
52. M. Waldeck-Weiermair, A. T. Deak, L. N. Groschner, M. R. Alam, C. Jean-Quartier, R. Malli, W. F. Graier, Molecularly distinct routes of mitochondrial $Ca^{2+}$ uptake are activated depending on the activity of the sarco/endoplasmic reticulum $Ca^{2+}$ ATPase (SERCA). *J. Biol. Chem.* **288**, 15367–15379 (2013).
53. U. De Marchi, C. Castelbou, N. Demaurex, Uncoupling protein 3 (UCP3) modulates the activity of Sarco/endoplasmic reticulum $Ca^{2+}$-ATPase (SERCA) by decreasing mitochondrial ATP production. *J. Biol. Chem.* **286**, 32533–32541 (2011).
54. T. S. Luongo, J. P. Lambert, A. Yuan, X. Zhang, P. Gross, J. Song, S. Shanmughapriya, E. Gao, M. Jain, S. R. Houser, W. J. Koch, J. Y. Cheung, M. Madesh, J. W. Elrod, The mitochondrial calcium uniporter matches energetic supply with cardiac workload during stress and modulates permeability transition. *Cell Rep.* **12**, 23–34 (2015).
55. T. S. Luongo, J. P. Lambert, P. Gross, M. Nwokedi, A. A. Lombardi, S. Shanmughapriya, A. C. Carpenter, D. Kolmetzky, E. Gao, J. H. van Berlo, E. J. Tsai, J. D. Molkentin, X. Chen, M. Madesh, S. R. Houser, J. W. Elrod, The mitochondrial $Na^+/Ca^{2+}$ exchanger is essential for Ca2+ homeostasis and viability. *Nature* **545**, 93–97 (2017).
56. A. M. Evangelista, M. D. Thompson, V. M. Bolotina, X. Tong, R. A. Cohen, Nox4- and Nox2-dependent oxidant production is required for VEGF-induced SERCA cysteine-674 S-glutathiolation and endothelial cell migration. *Free Radic. Biol. Med.* **53**, 2327–2334 (2012).
57. W. Ma, H. J. Sung, J. Y. Park, S. Matoba, P. M. Hwang, A pivotal role for p53: Balancing aerobic respiration and glycolysis. *J. Bioenerg. Biomembr.* **39**, 243–246 (2007).
58. M. Kobayashi, R. Nagashio, S. X. Jiang, K. Saito, B. Tsuchiya, S. Ryuge, K. Katono, H. Nakashima, E. Fukuda, N. Goshima, Y. Satoh, N. Masuda, M. Saegusa, Y. Sato, Calnexin is a novel sero-diagnostic marker for lung cancer. *Lung Cancer* **90**, 342–345 (2015).
59. D. Ryan, S. Carberry, Á. C. Murphy, A. U. Lindner, J. Fay, S. Hector, N. McCawley, O. Bacon, C. G. Concannon, E. W. Kay, D. A. McNamara, J. H. M. Prehn, Calnexin, an ER stress-induced protein, is a prognostic marker and potential therapeutic target in colorectal cancer. *J. Transl. Med.* **14**, 196 (2016).
60. C. Cardenas, M. Müller, A. M. Neal, A. Lovy, F. Jaña, G. Bustos, F. Urra, N. Smith, J. Molgó, J. A. Diehl, T. W. Ridky, J. K. Foskett, Selective vulnerability of cancer cells by inhibition of Ca(2+) transfer from endoplasmic reticulum to mitochondria. *Cell Rep.* **14**, 2313–2324 (2016).
61. J. Jung, P. Eggleton, A. Robinson, J. Wang, N. Gutowski, J. Holley, J. Newcombe, E. Dudek, A. M. Paul, D. Zochodne, A. Kraus, C. Power, L. B. Agellon, M. Michalak, Calnexin is necessary for T cell transmigration into the central nervous system. *JCI Insight* **3**, (2018).
62. R. Zhou, A. S. Yazdi, P. Menu, J. Tschopp, A role for mitochondria in NLRP3 inflammasome activation. *Nature* **469**, 221–225 (2011).
63. N. Myhill, E. M. Lynes, J. A. Nanji, A. D. Blagoveshchenskaya, H. Fei, K. C. Simmen, T. J. Cooper, G. Thomas, T. Simmen, The subcellular distribution of calnexin is mediated by PACS-2. *Mol. Biol. Cell* **19**, 2777–2788 (2008).
64. A. Wolmarans, B. Lee, L. Spyracopoulos, P. LaPointe, The mechanism of Hsp90 ATPase stimulation by Aha1. *Sci. Rep.* **6**, 33179 (2016).
65. J. Schindelin, I. Arganda-Carreras, E. Frise, V. Kaynig, M. Longair, T. Pietzsch, S. Preibisch, C. Rueden, S. Saalfeld, B. Schmid, J. Y. Tinevez, D. J. White, V. Hartenstein, K. Eliceiri, P. Tomancak, A. Cardona, Fiji: An open-source platform for biological-image analysis. *Nat. Methods* **9**, 676–682 (2012).
66. C. Ruiz-Canada, D. J. Kelleher, R. Gilmore, Cotranslational and posttranslational N-glycosylation of polypeptides by distinct mammalian OST isoforms. *Cell* **136**, 272–283 (2009).
67. E. Lucchinetti, A. E. Awad, M. Rahman, J. Feng, P. H. Lou, L. Zhang, L. Ionescu, H. Lemieux, B. Thébaud, M. Zaugg, Antiproliferative effects of local anesthetics on mesenchymal stem cells: Potential implications for tumor spreading and wound healing. *Anesthesiology* **116**, 841–856 (2012).
68. P. A. Srere, [1] Citrate synthase: [EC 4.1.3.7. Citrate oxaloacetate-lyase (CoA-acetylating)]. *Methods Enzymol.* **13**, 3–11 (1969).


**Acknowledgments:** We thank M. Michalak (University of Alberta) for the calnexin wild-type and knockout MEFs. We thank The Metabolomics Innovation Centre (www.metabolomicscentre.ca/) and Nanuc for metabolomic analyses. The GECO plasmids have been generously provided by R. E. Campbell (UofA). We thank T. Cali for the generous sharing of the SPLICS system. **Funding:** This study has been funded by CIHR operating grant MOP 133541 and NSERC grant RGPIN-2015-04105 to T.S. Funding for K.B. is provided by NSERC RGPIN-06484 and that for M.Z. is provided by a grant from the Heart and Stroke Foundation of Canada. Work by P.G.L. is supported by funding from NSERC (386803), CIHR (97870), and AIHS (200900500). J.S. is supported by the National Natural Science Foundation of China with grants 11675134 and 11874310. H.Q. is supported by the National Natural Science Foundation of China with grant 11504214. **Author contributions:** T.G. and T.S. designed the project. T.G., H.Q., M.C.Y., N.T., L.A.M., P.-H.L., P.M., and H.B. performed experiments. E.L. and M.Z. analyzed the oxymetry data. P.G.L. helped with ATPase analysis. N.T. and T.G. analyzed the electron microscopy data. P.M. and M.O. performed and analyzed the metabolomics data. H.B., S.B., and R.M. analyzed ATP levels within mitochondria. K.B. assisted with light microscopy. H.Q. and J.S. designed and executed mathematical modeling. T.G. and T.S. wrote the manuscript. **Competing interests:** The authors declare that they have no competing interests. **Data and materials availability:** All data needed to evaluate the conclusions in the paper are present in the paper or the Supplementary Materials. The plasmids encoding FLAG-tagged calnexin and calnexin knockout cell lines require a material transfer agreement from University of Alberta, Edmonton, Canada under the Uniform Biological Material Transfer Agreement (UBMTA).

Submitted 11 April 2019
Accepted 26 May 2020
Published 30 June 2020
10.1126/scisignal.aax6660

**Citation:** T. Gutiérrez, H. Qi, M. C. Yap, N. Tahbaz, L. A. Milburn, E. Lucchinetti, P.-H. Lou, M. Zaugg, P. G. LaPointe, P. Mercier, M. Overduin, H. Bischof, S. Burgstaller, R. Malli, K. Ballanyi, J. Shuai, T. Simmen, The ER chaperone calnexin controls mitochondrial positioning and respiration. *Sci. Signal.* **13**, eaax6660 (2020).

Science Signaling

# The ER chaperone calnexin controls mitochondrial positioning and respiration

Tomás Gutiérrez, Hong Qi, Megan C. Yap, Nasser Tahbaz, Leanne A. Milburn, Eliana Lucchinetti, Phing-How Lou, Michael Zaugg, Paul G. LaPointe, Pascal Mercier, Michael Overduin, Helmut Bischof, Sandra Burgstaller, Roland Malli, Klaus Ballanyi, Jianwei Shuai and Thomas Simmen

*Sci. Signal.* **13** (638), eaax6660.
DOI: 10.1126/scisignal.aax6660

**Calnexin as a metabolic nexus**

$Ca^{2+}$ flow from the ER to mitochondria promotes ATP production through oxidative phosphorylation. Gutiérrez *et al* . investigated the role of calnexin, an ER chaperone that interacts with SERCA, the ATPase that pumps $Ca^{2+}$ into the ER, in mitochondrial bioenergetics. The authors found that calnexin maintained SERCA in a redox state that was optimal for activity. Mitochondria were closer to the ER in cells without calnexin than in cells with calnexin. This enabled calnexin knockout cells to partially rescue Ca $^{2+}$ influx into mitochondria and to perform limited oxidative phosphorylation that was supplemented with increased glycolysis. These data suggest that calnexin positions mitochondria to regulate Ca $^{2+}$ flow from the ER and respiration.